RMZ

MATERIALS and GEOENVIRONMENT

MATERIALI in GEOOKOLJE

RMZ – M&G, **Vol. 68**, No. 1
pp. 1–50 (2021)

Ljubljana, December 2021

RMZ – Materials and Geoenvironment
RMZ – Materiali in geookolje
ISSN 1408-7073

Old title/Star naslov
Mining and Metallurgy Quarterly/Rudarsko-metalurški zbornik
ISSN 0035-9645, 1952–1997

Published by/Izdajatelj
Faculty of Natural Sciences and Engineering, University of Ljubljana/
Naravoslovnotehniška fakulteta, Univerza v Ljubljani

Associated Publisher/Soizdajatelj
Institute for Mining, Geotechnology and Environment, Ljubljana/
Inštitut za rudarstvo, geotehnologijo in okolje
Velenje Coal Mine/Premogovnik Velenje
Slovenian Chamber of Engineers/Inženirska zbornica Slovenije

Editorial Office/Uredništvo
Technical editors/Tehnična urednika Blaž Janc and Jože Žarn
Secretary/Tajnica Nives Vukič

Editorial Address/Naslov uredništva
RMZ – Materials and Geoenvironment
Aškerčeva cesta 12, p. p. 312
1001 Ljubljana, Slovenija
Tel.: +386 (0)1 470 46 10
Fax.: +386 (0)1 470 45 60
E-mail: bostjan.markoli@ntf.uni-lj.si
joze.zarn@ntf.uni-lj.si

Published/Izhajanje
4 issues per year/4 številke letno

Partly funded by Ministry of Education, Science and Sport of Republic of Slovenia./Pri financiranju revije sodeluje Ministrstvo za izobraževanje, znanost in šport Republike Slovenije.

Articles published in Journal "RMZ M&G" are indexed in international secondary periodicals and databases:/Članki, objavljeni v periodični publikaciji „RMZ M&G", so indeksirani v mednarodnih sekundarnih virih:
CA SEARCH® – Chemical Abstracts®, METADEX®, GeoRef.

Annual subscription for individuals in Slovenia: 20 EUR, for institutions: 30 EUR. Annual subscription for the rest of the world: 30 EUR, for institutions: 50 EUR/Letna naročnina za posameznike v Sloveniji: 20 EUR, za inštitucije: 30 EUR. Letna naročnina za tujino: 30 EUR, inštitucije: 50 EUR

Transaction account/Tekoči račun
Nova Ljubljanska banka, d. d., Ljubljana: UJP 01100-6030708186

VAT identification number/Davčna številka
24405388

Online Journal/Elektronska revija
https://content.sciendo.com/view/journals/rmzmag/rmzmag-overview.xml?result=4&rskey=iClOT4#

Table of Contents

Kazalo

Original scientific papers
Izvirni znanstveni članki

Original Scientific Article • DOI: 10.2478/rmzmag-2021-0001

Received: May 05, 2021
Accepted: August 16, 2021

Calibration of a 5x5 NaI(Tl) for Prompt In-Situ Gamma-ray Spectrometry System

Umerjanje 5x5 NaI(Tl) detektorja za in-situ sistem spektrometrije gama

Biere, P.E.[1,*], Aina, J.O.[2], Olaoye, M.O.[3], Mustapha, A.O.[2]

[1]Department of Physics, Niger Delta University, Wilberforce Island, Bayelsa State, Nigeria
[2]Department of Physics, Federal University of Agriculture Abeokuta, Ogun State, Nigeria
[3]Department of Physics, Lagos State University, Lagos State, Nigeria
*Corresponding author: E-mail: pbiere2003@gmail.com

Abstract in English

It is important to determine the presence of different radionuclides in the environment at all times in order to control and assess the risk level they pose to the environment. Laboratory and in-situ gamma-ray spectrometry can be used for detecting, monitoring, and assessing levels of radioactivity and radiation dose rates in the environment due to both natural and artificial sources. In this study, the greatest challenge in the calibration of detectors for in-situ gamma spectrometry has been solved. Calibration factors that can be used to convert the net count rates of collected spectrum's photopeak using a portable gamma-ray spectrometer, to quantitative specific activities have been derived. Calibration pads were simulated using standard materials RGU, RGK, and RGTh from International Atomic Energy Agency (IAEA). Region of interest (ROI) were carefully determined around these photopeaks in order to obtain count rates due to each radionuclide under its reference peak. The conversion factors obtained are reliable.

Keywords: Gamma ray spectrometry, NaI(Tl) detector, window analysis method, calibration factor

Abstract in Slovene

Določevanje prisotnosti različnih radionuklidov v okolju je pomembno z vidika nadziranja in ocenjevanja stopnje tveganja, ki ga predstavljajo za okolje. Laboratorijska in in-situ spektrometrija gama se lahko uporablja za odkrivanje, spremljanje in ocenjevanje ravni radioaktivnosti in stopnje sevanja v okolju, ki jih predstavljajo naravni in umetni viri. Največji izziv te raziskave je bilo umerjanje detektorja za in-situ spektrometrijo gama. Izpeljani so bili kalibracijski faktorji, ki jih je mogoče uporabiti za pretvorbo neto števila zbranih vrhov (photopeak) spektra z uporabo prenosnega spektrometra gama. Kalibracijske plošče so bile simulirane z uporabo standardnih materialov RGU, RGK in RGTh iz Mednarodne agencije za atomsko energijo (IAEA). Območja zanimanja so bila skrbno določena okoli teh vrhov (photopeak) z namenom pridobiti stopnje štetja za vsak radionuklid pod referenčnim vrhom. Dobljeni pretvorbeni faktorji so zanesljivi.

Ključne besede: spektrometrija gama, NaI(Tl) detektor, metoda analize okna, kalibracijski faktor

Introduction

Gamma ray spectroscopy system provides practical way to characterise dispersed radionuclides in or on the soil to ascertain possible changes in the environmental radioactivity. The gamma ray spectrometers generally used are made up of sodium iodide NaI(Tl) scintillation detectors or hyper pure Germanium (HPGe) detectors attached to multichannel analysers [1]. NaI(Tl) scintillation detectors are preferable because of their relatively high

efficiency and cheap maintenance but have the disadvantage of a poorer resolution [2].

Both laboratory and in-situ gamma spectroscopy are often used for detection, monitoring, and assessing levels of radioactivity and radiation dose rates in the environment due to both natural and artificial sources. Laboratory gamma spectroscopy systems have a more straightforward method of calibration while the calibration of an in-situ gamma spectroscopy system is a more rigorous process. In-situ gamma spectrometry has been used by many researchers including [3–6].

This study however seeks to derive empirical calibration factors that can be used to convert the net count rates of collected spectrum's photopeak, obtained using a portable gamma-ray spectrometer, to quantitative specific activities. This work therefore is aimed at solving the greatest challenge involved in the calibration of detectors for in-situ gamma spectrometry [7].

Materials and methods

The gamma-ray spectrometer used in this study is portable 5 × 5 NaI(Tl) scintillation detector which has a gain that is sensitive to change in temperature and magnetic fields in its immediate surroundings. It consists of combined Amplifier-Voltage supply, an ORTEC Multipurpose Analyser (MCA), and a Multichannel Buffer (MCB), which performs data acquisition and analysis. It also consists of a digiBase, which is a 14-pin photomultiplier tube base for the gamma-ray spectroscopy applications with a NaI(Tl) scintillation detector. It combines a miniaturised preamplifier and detector high voltage, 0 V to +1,200 V bias, with a powerful digital multichannel analyser and special features for fine time-resolution measurements. It is supplied with MAESTRO-32 MCA Emulation Software, which contains all that is necessary to control and to adjust the acquisition parameters, acquire the data, and save the spectra [8]. The digiBASE also incorporates a gain stabiliser to significantly diminish the sensitivity of the detector [9]. It works by monitoring the centroid of a designated peak in the energy spectrum; the fine gain is automatically and continuously adjusted to maintain the centroid of the peak at its desired position.

The calibration of portable gamma ray spectrometers for the use of natural radioactivity measurements is done most times by the use of standard spectra that are obtained using at least three concrete pads enriched in K, U, and Th, and another that is pad free of radioactivity is used to represent the background [10, 11]. These pads are usually at least 2 m^2 in area and 0.5 m thick [12]. The design of an ideal pad enriched with one radionuclide inside and a perfect homogeneous distribution of the radioisotopes in its volume tend to be expensive and nearly unrealistic; hence, a simpler customised and applicable procedure was adopted. There are two calibration steps used to determine the performance of the detector. First is the energy calibration, which is the procedure that made it possible to interpret the acquired spectrum as a function of the energy associated with the events of decay. This is a function of the concentration of radioactive elements present in the system under analysis. The second stage in the calibration process was the determination of the factors that related the count rate under a photopeak to soil radioactivity concentration ($BqKg^{-1}$) of the radionuclide and dose rate in air.

Energy calibration

Energy calibration of the detector was performed by weighing the standard materials, RGU, RGK, and RGTh, from the International Atomic Energy Agency (IAEA) in petri dishes. Total masses of 144.00 g, 183.90 g, and 130.02 g of RGU, RGK, and RGTh, respectively, were used. The standard materials in the petri dishes were arranged to depict the inhomogeneous distribution of the radionuclide in the environment. The detector was placed directly above the arrangement at a height of 140 mm. This was allowed because as much as possible only the natural radioactivity, as a result of the low gamma emitting radionuclides present in the soil, was intended to be captured. The Window Analysis Method (WAM) was applied as spectrum analysis method. In this method, only the region of interest of the spectrum is considered [10]. The assessment of the concentration of Potassium was therefore done by studying the single peak emitted

by ^{40}K at the energy of 1,460 keV, Uranium, ^{238}U was at the energy of 1,765 keV from ^{214}Bi, while Thorium, ^{232}Th, was through the gamma rays of ^{208}Tl with energy equal to 2,614 keV. After a preset time of 300 s [13], a spectrum was captured, and the channels of the various photopeaks corresponding to the gamma energies were identified. Figure 1 shows the spectrum as captured during the experiment. The photopeaks of interest were 295 keV, 1,120 keV, and 1,765 keV. The calibration procedure continued with the selection of the calibration option of the software and inserting the gamma energies of each of the peaks of interest against their channel numbers. A relation of the gamma energy versus the channel number was thus established by the software. The regions of interest (ROI) were carefully determined around these photopeaks in order to obtain count rates due to each radionuclide under its reference peak. These count rates were converted to soil activity concentration of the radionuclides using the conversion factors.

Efficiency calibration

The pulse height distribution that was obtained earlier from the detector and MCA only informs us about the distribution of energy depositions in the active volume of the detector. In order to do a radionuclide-specific quantification of the activity, efficiency calibration linking the number of recorded counts in the detector to the ground deposition activity level is required [14]. According to [15], the number of counts per second, N_f, obtained under a photopeak due to a particular gamma energy, E, is related to the soil radioactivity concentration, A of the radionuclide producing the peak by Equation 1 [16].

$$\frac{N_f}{A} = \frac{N_f}{N_o}\frac{N_o}{\varnothing}\frac{\varnothing}{A} \quad (1)$$

In Equation 1, $\frac{N_f}{A}$ is the photopeak count rate at the gamma energy per unit activity concentration of the radionuclide in the soil ($\frac{cps}{Bqkg^{-1}}$), $\frac{N_f}{N_o}$ is the angular correction factor, which accounts for the nonuniformity of the detector response to gamma rays incident at varying angles, $\frac{N_o}{\varnothing}$ is the on-axis response of the detector (normal to detector face) given in the count rate per uncollided

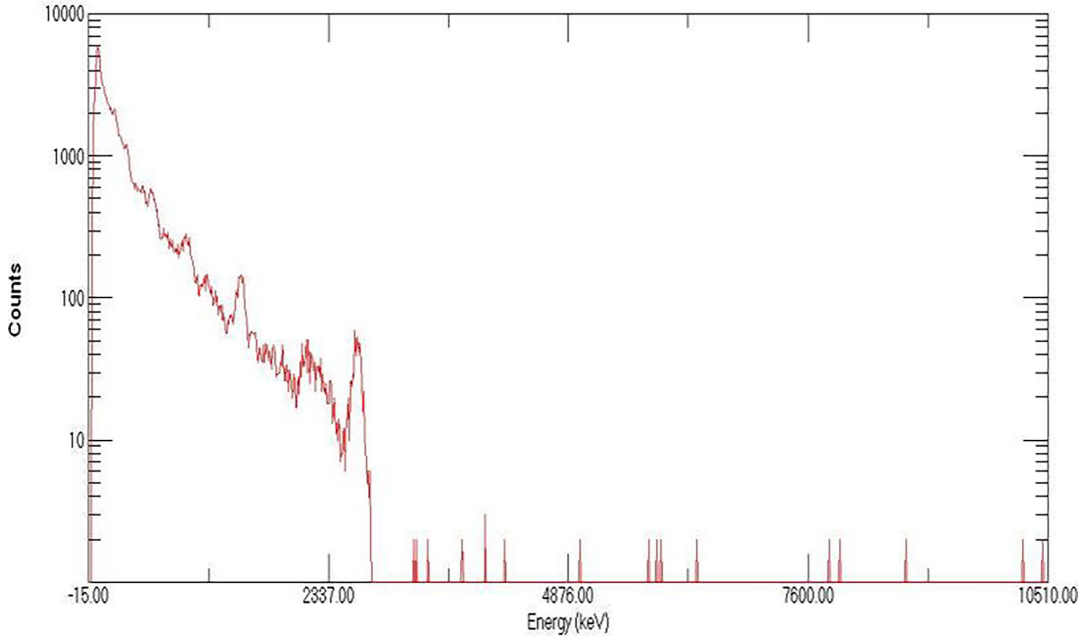

Figure 1: *Spectrum obtained during calibration showing gamma lines of the primordial radionuclides.*

flux of parallel gamma rays ($\frac{cps}{\gamma m^{-2}s^{-1}}$), $\frac{\varnothing}{A}$ represents the total uncollided flux per unit source activity concentration ($\frac{\gamma m^{-2}s^{-1}}{Bqkg^{-1}}$), and $\varnothing$ is the gamma r y unscattered flux on the detector ($\gamma m^{-2}s^{-1}$).

Determination of calibration factors

The factor $\frac{N_o}{\varnothing}$ represents the response of the detector to photons at normal incidence. Its value was determined by placing the uranium standard material (RGU-1) obtained from the International Atomic Energy Agency (IAEA) at a distance of 140 mm from the detector face. After a preset counting time of 300 s, a spectrum was obtained. Figure 1 is the spectrum showing the response of the detector to the associated radionuclide with the photopeaks of interest, with 1,460 kev for ^{40}K, 1,764 kev for ^{226}Ra, and 2,615 kev for ^{232}Th. A region of interest was carefully marked around the photopeaks so that the count rate, N_o, was obtained. The flux $\varnothing$ was determined by using Equation 2 [16].

$$\varnothing = \frac{A \times \gamma}{4\pi R^2} \qquad (2)$$

Here γ is the gamma yield at a particular gamma energy, *R* is source to detector distance (m), and A is radiation source activity ($Bqkg^{-1}$).

$\frac{N_f}{N_o}$ was determined from count rate under photopeaks obtained by moving the standard source from 0^0–50^0 in steps of 10^0. If $\frac{N_f(E,\theta)}{N_o}$ is the ratio of the detector response to gamma ray of energy *E*, at angle, θ, with respect to the response at θ= 0^0, then $\frac{N_f}{N_o}$ can be determined using Equation 3 [15].

$$\frac{N_f}{N_o} = \frac{1}{\varnothing}\int_0^{\pi/2} \varnothing(\theta)\frac{N_f(E,\theta)}{N_o}d\theta \qquad (3)$$

The determination of $\frac{N_f}{N_o}$ can be achieved by numerically integrating Equation 3 (Jibiri and Farai, 2005). The integration was performed in this work by using the experimental values of $\frac{N_f(E,\theta)}{N_o}$ and the value of $\varnothing$. By substituting the values of $\frac{N_o}{\varnothing}$, $\frac{N_f}{N_o}$, and $\frac{\varnothing}{A}$ in Equation 1, the desired conversion factor $\frac{N_f}{A}$ is obtained.

Determination of in-situ background

A body free from the presence of any radionuclide was simulated. This was achieved by putting distilled water into a fairly large bathtub to attenuate the natural background gamma rays. The in-situ gamma spectrometer was mounted on the water body, and counting was done for a preset time of 300 s. A spectrum was captured, and the count rate under the photopeaks of ^{40}K, ^{226}Ra, and ^{232}Th were determined by carefully taking the region of interest, ROI, around the photopeaks.

Results and discussion

Table 1 presents the results of calibration of the detector used in this work for in-situ gamma spectrometry using the window analysis method. The calculated values of the conversion factor, $\frac{N_f}{A}$, obtained here can be used for in-situ gamma-ray spectrometry.

Conclusion

The in-situ gamma spectrometer has been properly calibrated and can be deployed for radiation detection, measurement, characterisation as well as for emergency response assessments. The calibration procedure developed in this work for the in-situ gamma-ray spectrometer is reliable, cost effective, and realisable. It has equally given reliable conversion factors for the

Table 1: *In-situ conversion factors.*

Radionuclide	$\frac{N_o}{\emptyset}\left(\frac{cps}{\gamma m^{-2}s^{-1}}\right)$	$\frac{\emptyset}{A}\left(\frac{\gamma m^{-2}s^{-1}}{Bqkg^{-1}}\right)$	$\frac{N_f}{N_o}$	$\frac{N_f}{A}\left(\frac{cps}{Bqkg^{-1}}\right)$
^{40}K	0.013	0.433	0.895	0.005
^{238}U	0.008	0.616	1.647	0.008
^{232}Th	0.001	1.451	1.045	0.002

5 x 5 NaI(Tl) detector, which can be used for prompt detection of gross contamination in the environment.

Acknowledgements

The authors would like to express their appreciation for the efforts of Mr. Olagbaju Peter and Dr. Ogunremi in obtaining baseline data for this study.

References

[1] Faanu, A. et al., 'Calibration and Performance Testing of Sodium Iodide, NaI (Tl), Detector at the Food and Environmental Laboratory of the Radiation Protection Institute of the Ghana Atomic Energy Commission', *West African Journal of Applied Ecology*, no. 19, 2011, pp. 39–52.

[2] Papastfanou, C., 'Measurement of Naturally Occurring Radionuclides with Several Detectors: Advantages and Disadvantages', *Austral-Asian Journal of Cancer*, vol. 7, no. 4, 2008, pp. 267–280.

[3] Arogunjo, A.M., Faria, I.P., Jibiri, N.N., 'Comparison of In-Situ and Laboratory Gamma-Ray Spectroscopy of Terrestrial Gamma Radiation in Ibadan, South Western Nigeria', *Global Journal of Pure and Applied Sciences*, vol. 8, no. 4, 2002, pp. 505–509.

[4] Wang, N. et al., 'Determination of Radioactivity Level of ^{238}U, ^{232}Th and ^{40}K, in Surface Medium in Zhuhai City by In-Situ Gamma-Ray Spectrometry', *Journal of Nuclear Science and Technology*, vol. 42, no. 10, 2005, pp. 888–896.

[5] Jibiri, N.N., Farai, I.P., 'Application of In-Situ Gamma-Ray Spectrometry in the Determination of Activity Concentration of ^{40}K, ^{238}U and ^{232}Th and Mean Annual Effective Dose Rate Levels in Southeastern Cities in Nigeria', *Radioprotection*, vol. 40, no. 4, 2005, pp. 489–501.

[6] Obasi, I.A. et al. 'In-Situ Measurement of Radionuclide Concentrations (^{238}U, ^{40}K, ^{232}Th) in Middle Cretaceous Rocks in Abakiliki-Ishiagu Area, Southeastern Nigeria', *Arabian Journal of Geoscience,* no. 13, 2020, pp. 1–9, DOI: 10.1007/s12517-020-05360-4.

[7] Benke, R.R., Kearfott, K.J., 'Comparison of In-Situ and Laboratory Gamma Spectroscopy of Natural Radionuclides in Desert Soil', *Health Physics Society*, vol. 73, no. 2, 1997, pp. 350–361.

[8] ORTEC, *Revision D. DigiBase User's Manual*, Advance Manual Revision Measurement Technology Inc., 2014, 931003.

[9] Pilakouta, M. et al., 'A Methodology for Expanding the Use of NaI(Tl) Based Spectrometry in Environmental Radioactivity Measurements', *Applied Radiation and Isotopes,* no. 139, 2018, pp. 159–168.

[10] Hendricks, P.H.G.M., Limburg, J., de Meijer, R.J., 'Full-Spectrum Analysis of Gamma-Ray Spectra', *Journal of Environmental Radioactivity*, no. 53, 2001, pp. 365–380.

[11] Lovborg, I. et al., 'Pad Facility for the Calibration of Gamma-Ray Measurements on Rocks', Roskilde, Denmark, Riso National Laboratory, 1981,

[12] IAEA, *Radiological Accident in Goinia*, IAEA-ST1/PUB/847, Vienna, IAEA, 1990.

[13] Miller, K.M., *Field Gamma-Ray Spectrometry HASL–300*, 28th edn., Section 3 vol. 1. 1997.

[14] Jonas, B.,)'Improving Accuracy of In-Situ Gamma-Ray Spectrometry', *Print and Media*, 2008, p. 2,004,940.

[15] Beck, H.L., DeCampo, J., Gogolak, C. *In-Situ Ge(Li) and Na(Tl) Gamma-Ray Spectrometry*, New York, U.S. Department of Energy, Environmental Measurements Laboratory HASL-258, 1972.

[16] Miller K.M, Shebell P. *In Situ Gamma-Ray Spectrometry: A Tutorial for Environmental Radiation Scientists*, New York, Environmental Measurements Laboratory, U.S. Department of Energy, 1993.

Original Scientific Article • DOI: 10.2478/rmzmag-2021-0002

Received: June 22, 2021
Accepted: July 02, 2021

Copper tailings reprocessing

Pridobivanje bakra z deponij

Damjan Hann*
University of Ljubljana, Faculty of Natural Sciences and Engineering, Department of Geotechnology, Mining and Environment, Aškerčeva 12, Ljubljana, Slovenia
*Corresponding author: E-mail: damjan.hann@ntf.uni-lj.si

Abstract in English

Copper is widely used in the modern world. An excellent conductor of electricity, it is used in the electrical industry, in the construction industry because of its good corrosion resistance, and in the manufacture of heat exchangers in heating and cooling systems owing to its excellent thermal conductivity. Copper production has increased throughout the twentieth century, and this trend has continued over the last twenty years. The demand for copper is expected to increase significantly by the year 2030. Owing to the high prices of this metal and the lack of deposits, part of the demand can be met by extraction from copper-bearing tailings. In the past, owing to the lower level of technological development and lower copper prices, materials comparable in copper content to the copper ores mined today have ended up in tailings. Since these are already processed materials, the costs of mining, crushing and milling are largely eliminated, making them promising raw materials. The article presents the technological possibilities of reprocessing and also estimates the amount of copper that could be obtained worldwide in this way.

Keywords: tailings reprocessing, multi-gravity separator, flotation, copper

Abstract in Slovene

Baker v sodobnem svetu masovno uporabljamo. Kot odličen prevodnik električne energije je uporaben v elektro industriji, zaradi dobre odpornosti na korozijo v gradbeni industriji, zaradi odlične toplotne prevodnosti pa se ga uporablja za izdelavo toplotnih izmenjevalcev v ogrevalnih in hladilnih sistemih. Proizvodnja bakra je naraščala celotno dvajseto stoletje, trend pa se nadaljuje tudi v zadnjih dvajsetih letih. Do leta 2030 se pričakuje precejšnja rast povpraševanja po bakru. Zaradi visokih cen te kovine in pomanjkanja nahajališč je možno del potreb pokriti s pridobivanjem na jaloviščih, ki vsebujejo baker. V preteklosti so namreč zaradi nižje stopnje tehnološke razvitosti in nižjih cen bakra na jaloviščih končali materiali, ki so po vsebnosti bakra primerljivi z bakrovimi rudami, ki se odkopavajo danes. Glede na to, da gre za že procesirane materiale, stroški rudarjenja, drobljenja in mletja večinoma odpadejo, zato gre za zelo perspektivne surovine. V članku so predstavljene tehnološke možnosti glede reprocesiranja, ocenjena je tudi količina bakra, ki bi jo lahko na ta način pridobili globalno.

Ključne besede: reprocesiranje jalovišč, multi-gravitacijski separator, flotacija, baker

Introduction

In the past, prices for various non-ferrous metals were somewhat lower than they are today, and this is the main reason why the mining industry left significant amounts of those metals in tailings dams around the world. The prices of non-ferrous metals simply did not allow for too much engagement when it came to mineral processing and ore beneficiation. The second, equally important reason for the low efficiency of ore processing was the equipment, which was not as advanced as it is today.

Copper is considered one of the first metals ever mined and used by mankind, and it has contributed significantly to the improvement

of society since the beginning of civilization [1]. More specifically, copper is a metal that has been in use for about 10,000 years [2], and there is no indication that it will be replaced by a similar material in the near future. The price of copper has recently peaked as concerns about supply disruptions and strong demand have raised expectations of a tight market. This key energy transition metal, which is also widely used in construction, is trading at around $10,000 a ton. The price is at its highest level since July 2011, when copper traded at about the same price. Analysts at Goldman Sachs expect copper prices to reach $15,000 per ton in 2025, driven by high demand, which is forecast to grow by almost 600% by 2030. The projected demand is likely to lead to a supply deficit and higher copper prices, which in turn are likely to trigger new investment cycles [3].

Notwithstanding the fact that copper has been used by humans for 10,000 years, as shown in Figure 2, a negligible amount of copper was mined before 1900. About half of the total amount of copper was produced by 1998, while another half was mined in the last 22 years. Total copper production from 1900 until the end of 2020 was about 740 million tons [5, 6].

In a situation in which global copper demand is growing and copper prices are steadily increasing, reprocessing copper tailings is becoming an increasingly logical decision [7, 8, 9]. In most of the copper tailings deposited in the last century, there is a sufficiently high content of valuable components so that the tailings can be economically exploited and considered a potential future resource [10].

Nowadays, the development of new technologies allows the exploitation of copper, which in the past was disposed of together with the tailings due to inefficient copper extraction processes. Another reason that enables the exploitation of copper tailings is the high price of copper on the world market. In the past, tailings, now considered a valuable source of metals, were treated as waste due to the low price of copper.

In the last century, the copper content of some tailings was as high as 0.75%, which means that these historic tailings may have a higher content than the current deposits, which mostly contain 0.2%–0.8% copper. However, as each individual deposit is at least a little different from all the others, and consequently so is the tailings dam, it is impossible to predict in advance the optimal procedure for reprocessing [7].

A significant and, above all, positive side effect of tailings reprocessing is the protection of the environment by eliminating or at least reducing exposure to hazardous substances.

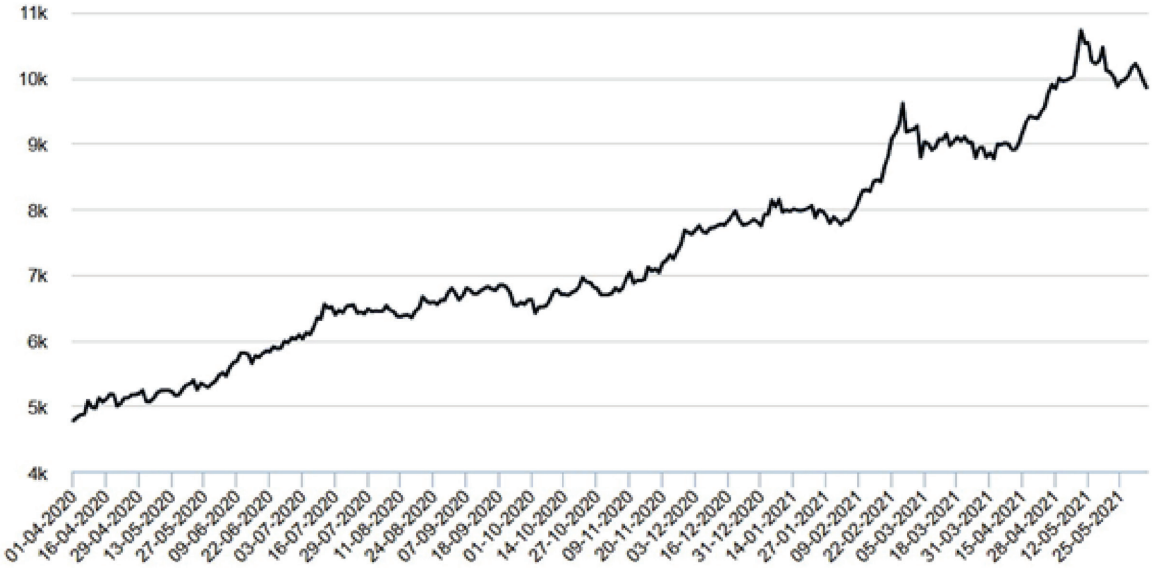

Figure 1: *Copper price on the London Metal Exchange since April 2020 (USD/t) [4].*

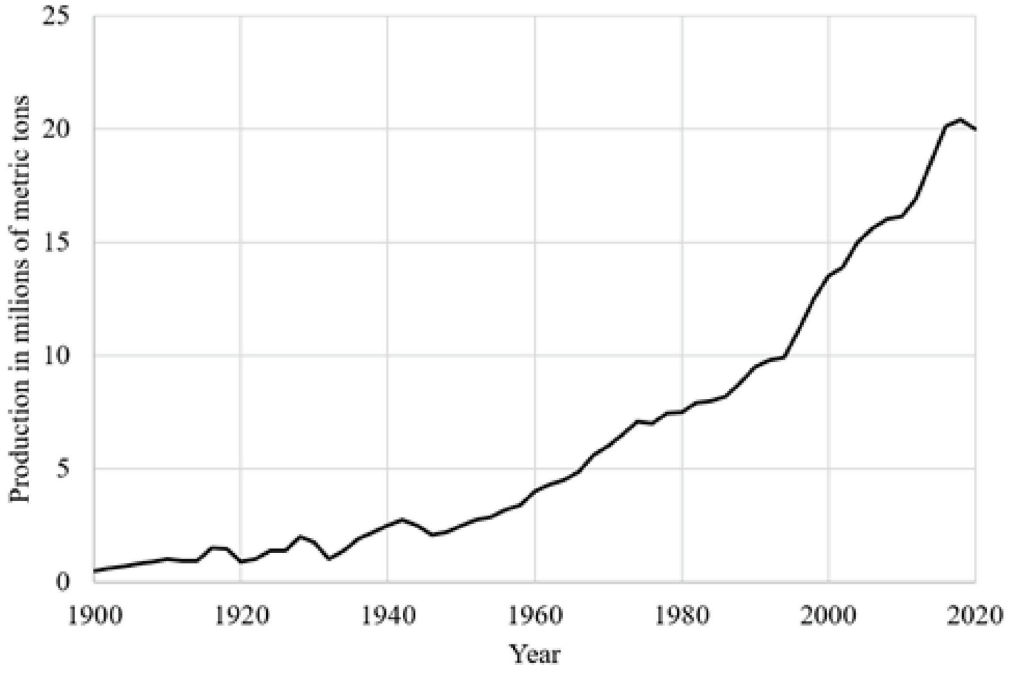

Figure 2: *Total copper mine production worldwide from 1900 to 2020 (adapted from [5, 6]).*

The economic balance of tailings reprocessing can also be improved through environmental protection if a government or community is interested in rehabilitating an area degraded by tailings and is willing to allocate funds to such a project. If heavy metals and other potentially harmful substances are removed from the material, the sale of the remaining material for everyday use in mass consumption can also be considered.

Since the material in the tailings dams is already accumulated in large quantities and has undergone mining and certain mineral processing such as crushing and grinding of the original ore, the costs are expected to be lower than those associated with extracting metals from the deposits.

In the exploitation of deposits, mining represents the highest cost [10] and together with the costs of crushing and milling in the case of a 100,000 t/day copper concentrator (Table 1), mining costs represent the largest part of all costs.

Owing to the many advantages of tailings retreatment, several tailings retreatment plants are already in operation around the world [10], and many more are expected to start producing copper in the near future.

Table 1: *Approximate relative costs of a 100,000 t/day copper concentrator [10].*

Item	Cost (%)
Crushing	2.8
Grinding	47.0
Flotation	16.2
Thickening	3.5
Filtration	2.8
Tailings	5.1
Reagents	0.5
Pipeline	1.4
Water	8.0
Laboratory	1.5
Maintenance support	0.8
Management support	1.6
Administration	0.6
Other expenses	8.1
Total	100

If metal minerals are to be extracted from ore or tailings, there are several chemical options. Minerals can be subjected to pyrometallurgy, which involves exposure to high heat; hydrometallurgy, which requires solvents; or electrometallurgy, which uses high electrical power, although combinations of different processes are also possible. By far the most common process among those mentioned is pyrometallurgy – or more specifically, smelting. All these processes are otherwise quite energy intensive. This is the main reason why smelting is not carried out until the copper ore has been concentrated to the maximum by mineral processing procedures, eg up to 25%. This also reduces transportation costs. Physical processes for separating valuable and gangue minerals are the exact opposite of chemical processes in terms of energy input [10].

This article presents various technological options for exploitation of tailings, which are expected to be rich enough in copper, according to the current copper price. It also reports the results of feasibility tests on the economic extraction of copper from tailings and gives an estimate of the amount of copper that could be extracted from tailings worldwide.

The idea for the research was triggered by the rising prices of non-ferrous metals, which made tailings reprocessing interesting. Large copper mines operating in the last century with the technology available at the time could not be as effective, so the copper content in tailings is likely to be high enough to be seen as a promising opportunity. Any feasibility testing or, in other words, demonstration of the viability of tailings should start with samples collected in the field. This should be followed by granulometric analysis and compositional analysis, for example XRF (X-ray fluorescence) analysis. Finally, enrichment of copper content using appropriate equipment, such as a multi-gravity separator or flotation cell, and redetermination of the composition of the tailings should follow.

Materials and methods

In copper mining, the concentration of ore is usually accomplished by a process called froth flotation [11], in which the valuable substance floats to the surface with the aid of air bubbles. Unwanted material, called gangue, sinks to the bottom and is removed. The concentration process can also be carried out using a variety of different techniques and technologies, including gravity-based methods, leaching, dense liquid separation, etc.

Sampling

In the past, many underground and open pit copper mines were in operation in Europe, so several sites with tailings dams are available for research purposes [12, 13]. Sampling was carried out at a tailings dam that had been created and filled in the second half of the previous century. Owing to the time period in which the tailings dam was formed, the copper content in the original ore, and the technology available at the time of copper extraction, the samples collected represent typical material suitable for copper tailings reprocessing. An excavator was used to obtain representative samples [14]. As it is characteristic for most bulk materials exposed to external forces over an extended period of time, oxidation occurred. Excavation of the material revealed that the material layers at a depth of about 1.5 meters and deeper are grey in colour and are not oxidised. Within the layers near the surface, the proportion of material that has been exposed to weathering increases, and there is a gradual transition in the colour of the tailings from grey to brown. In some cases, intact material occurs at depths as shallow as 0.5 meters. Samples were taken from both layers, and the total amount of almost one tonne of material was transported to the laboratory for examination.

The content of copper in the samples was determined by X-ray fluorescence (XRF), a technique that determines the presence of individual elements in a sample without damaging it. Samples of upper oxidised material and bottom unoxidised material were analysed separately for element content. It was found that the copper content in the samples taken from the upper part of the tailings was much lower than in the unoxidised samples, for which an average of 0.16% copper content was measured. As reported in [7], there is a reprocessing plant in Chile that extracts copper from tailings grading 0.12% to 0.27% Cu. Oxidised samples were

consequently identified as not promising for reprocessing. The lower copper content in the upper layers is due not only to the weathering of the particles, but also to the continued downward movement of the heavier grains with water currents. Grains with a higher density, such as grains with some copper content (copper density is about 9 g/cm^3), definitely belong to this group of grains.

Granulometric analysis

Since the applicability of each method in mineral processing is highly dependent on particle size, granulation analysis was performed. Sieve analysis was carried out using seven different standard laboratory sieves [15] with aperture sizes: 32, 71, 125, 250, 500, 1,000 and 2,000 μm [14]. Before sieving, homogenisation, sampling [16] and drying of the appropriate amount of the tested material was performed. Table 2 shows the results of sieving analysis. The results and the graphical representation in Figure 3 show that the parameter d_{50} – mean particle size – is about 200 μm, while d_{90} is in the range of 450 to 500 μm.

Multi-gravity separator

Multi-gravity separators are separation systems that can be useful in applications such as upgrading industrial minerals, recovering precious metals, and recovering metal minerals such as copper minerals. They have proved their usefulness by enabling the production of high-grade concentrates at high recovery from low-grade tailings [10, 14, 17, 18].

As long as there is a sufficient difference in the specific gravity of the grains, this machine can separate a particular mineral or group of heavy minerals from a low-density gangue within a liquid suspension. For effective separation, there should be at least one SG (specific gravity) unit between the heavy and light particles. Nowadays, laboratory versions of multi-gravity separators up to full-scale industrial units with an ore processing capacity of 5 t/h are available on the market, which can treat even ultrafine particles down to a size of 1 μm.

The invention and further development of the multi-gravity separator, also known as an enhanced gravity separator, was inspired by a conventional shaking table. The physical basis and operating principle of both concentrators are quite alike. In the multi-gravity separator, centrifugal forces are used to increase the efficiency of separation of fine and ultra-fine particles. The centrifugal force acting on the grains is, in absolute value, much higher than the force of gravity in case of conventional shaking table; therefore, separation is easier to achieve. The forces acting on the particles can even reach up to 15 g and more.

Separately prepared and constantly stirred homogeneous feed slurry enters at the centre of the rapidly rotating conical drum. As shown in

Table 2: *Results of sieve test.*

Aperture size (μm)	Size interval (μm)	Sieve mass (g)	Cumulative pass (g)	Cumulative pass (%)	Cumulative oversize (%)
2,000	+2,000	13	2.81	97.19	2.81
1,000	1,000–2,000	4	0.86	96.33	3.67
500	500–1,000	11	2.38	93.95	6.05
250	250–500	143	30.89	63.06	36.94
125	125–250	193	41.68	21.38	78.62
71	71–125	54	11.66	9.72	90.28
32	32–71	24	5.18	4.54	95.46
0	0–32	21	4.54	0.00	100.00

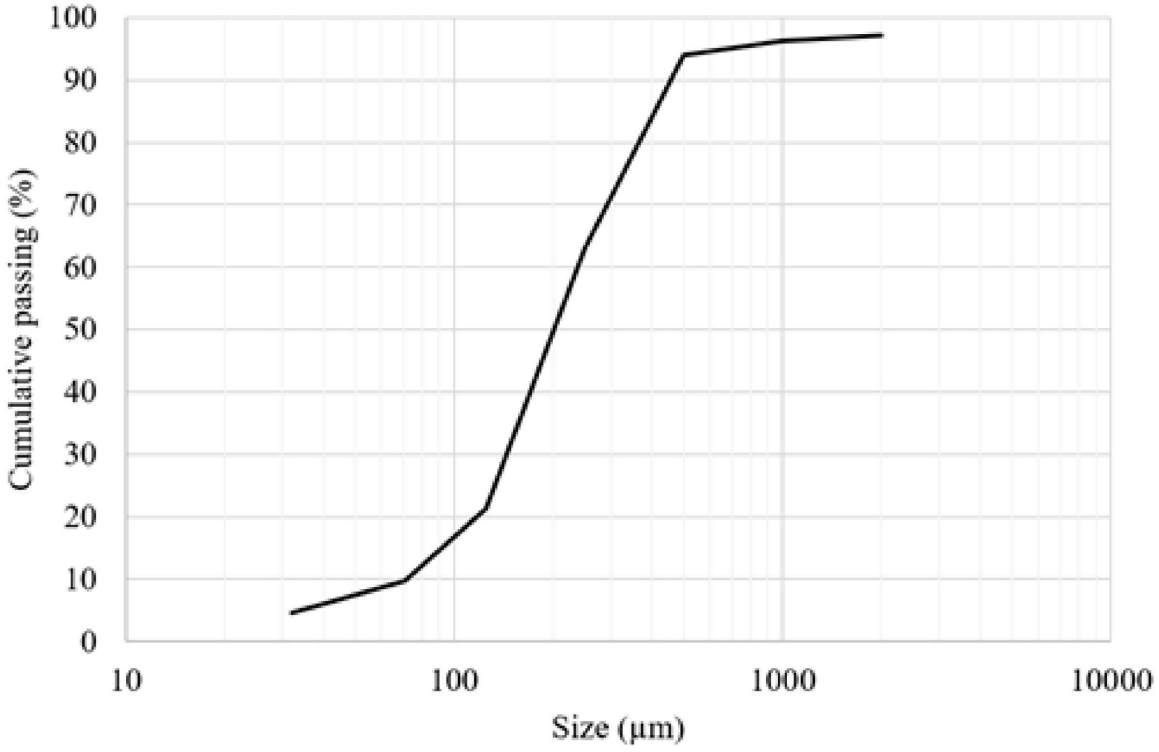

Figure 3: *Graphical interpretation of the sieve test.*

Figure 4, the drum rotates clockwise whilst being shaken by cyclic oscillation in the horizontal direction at 4–6 cps. After a few turns, the entering slurry is spread evenly over the entire surface on the inside of the drum. The light fractions begin to collect in the thin flowing film of water, which continuously ensures the movement of these particles in the direction of the far end of the drum. Particles with higher density are affected by the high centrifugal forces or so-called enhanced gravity and shear forces due to shaking. Consequently, they are squeezed through the pulp film and end up as pressed to the drum. The further movement of the heavy particles is controlled by the unique scraper system. Rotating scrapers direct heavy grains within the semi-solid layer to the concentrate outlet, which is in the opposite direction as the fine grains are discharged. The scrapers also rotate clockwise like the drum but at a slightly higher rpm (revolutions per minute).

Small quantities of wash water are added through the wash water inlet, which is located close to the concentrate outlet. The purpose of the wash water is to create a water film capable of carrying and bringing out the entrained light fraction into the tailings outlet and rinsing the dense grains just before they are discharged from the concentrator.

Flotation

The extent to which useful substance is lost to tailings during ore processing determines whether or not a deposit can be economically exploited. The proportion of losses depends partly on the natural characteristics of the ore deposit and partly on the technology used for extraction. More specifically, the losses depend, on the one hand, on the spatial distribution of the minerals in the ore and the mineralogy itself, and on the other hand, on the efficiency of the concentration [10]. As with other methods, technological progress in flotation brings new opportunities for the reprocessing of low-grade copper tailings.

Flotation is a process in which a useful substance is separated using chemical reagents in a three-phase system (solid, liquid and gas) by combining the grains with air bubbles to obtain a froth of concentrate as the tailings sink to the bottom.

The main problem with the flotation of tailings is the fact that the material has already been processed – crushed and milled – so that

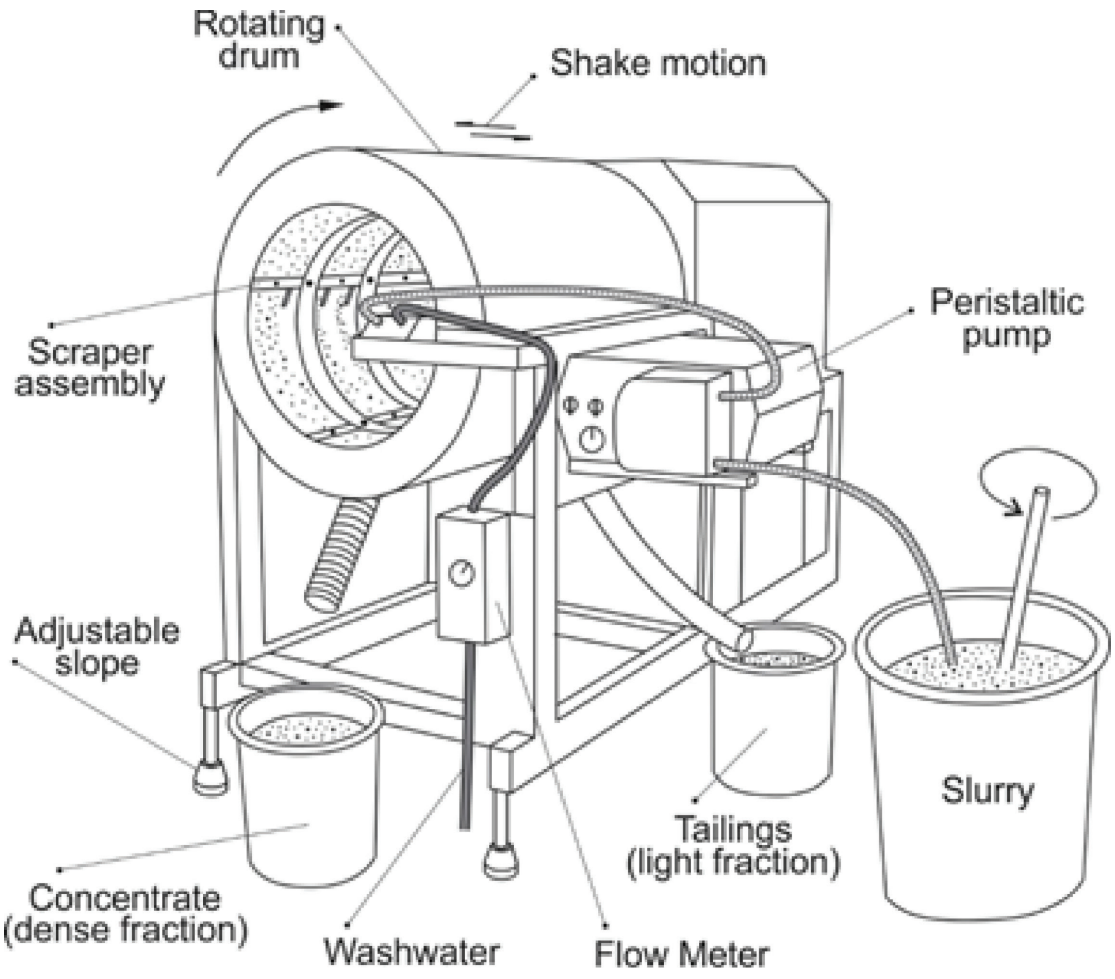

Figure 4: *Multi-gravity separator – MGS (adapted from [10, 14, 18]).*

the majority of particles are smaller than 100 or even 50 microns. Many different problems can arise in the flotation of such fine fractions, and the smaller the particles, the greater the problems. Particles with 1 mm^3, milled to 1 μm^3 particles, mean a huge increase in the number of bubbles required. In this case, the possibility of each particle being associated with an air bubble is small. Another problem is the huge increase in the amount of reagents required due to the increase in the specific area [7]. Therefore, if the particles in the tailings are very small, a method other than froth flotation should be used, based on a different physical basis.

Results and discussion

Since the multi-gravity separator (MGS) has many adjustable parameters, it is quite a challenge to find an optimal combination for a quality separation. Operating variables of the MGS are:

— shake amplitude
— shake frequency
— drum rotational speed
— drum angle of inclination
— wash water flow rate
— feed percent solids

During the test, the drum rotational speed, solids concentration, and wash water flow rate were adjusted while the other parameters remained constant. After each individual test, which lasted approximately five minutes, a small amount of concentrate was taken, and then a series of samples were heated to dryness. This was followed by elemental composition measurements, which showed that the combination of adjustable parameters plays a significant role when MGS is used for separation.

The upgrade factor, which is the relationship between the share of copper in the concentrate and the share of copper in the feed material, can be as low as close to 1. However, the concentration of copper when optimal conditions were reached was several times higher compared with the concentration in the feed material [14].

Tests with the MGS gave solid results, but to get even better results, the processing of the material with the multi-gravity separator would have to be combined with another physical process. Since today's knowledge of flotation far exceeds what we knew about this process decades ago, the flotation process could be used especially for coarser fractions.

Figure 5 shows the cumulative size distribution of the material from the copper tailings reprocessing plant in Chile, which has a d_{90} of 270 µm and was successfully processed in the flotation circuit [7]. Since the material considered in this work is quite similar in size to that processed in Chile, it would be useful to perform an additional test with flotation cells. Moreover, a batch process can be used.

From the combination of all the information obtained from the experiments and the information provided by other researchers on copper reprocessing, it can be concluded that the process line shown in Figure 6 would be successful for a tested material.

Taking into account the quantities of copper produced with low efficiency during the last century, the amount of material accessible on tailings dams, the oxidation of tailings, the efficiency of copper reprocessing and the average copper content within tailings, it is possible to give an estimate [Equation (1)] of the capacity of copper that can be recovered from tailings worldwide:

$$P = TP \times a \times b \times c \times d \times e \times f \quad (1)$$

P = 737 million tons × 0.5 × 0.33 × 0.8 × 0.8 × 0.75 × 0.97 = cca 57 million tonnes
where the following abbreviations are used:

P: global potential of mining tailings for copper production
TP: total global historical production of copper
a: share of low-efficiency copper production, characteristic for the last century
b: ratio of copper content in original ore to copper content in tailings
c: share of tailings dams accessible for reprocessing

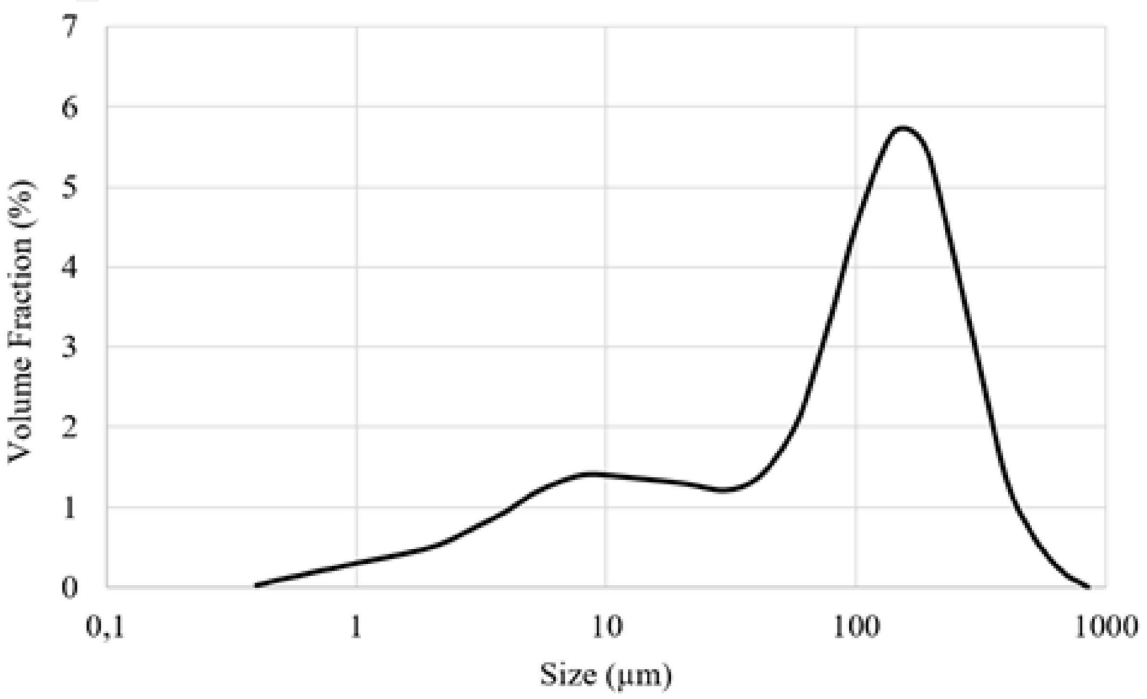

Figure 5: *Cumulative size distribution of feed material from a copper tailings reprocessing plant (adapted from [7]).*

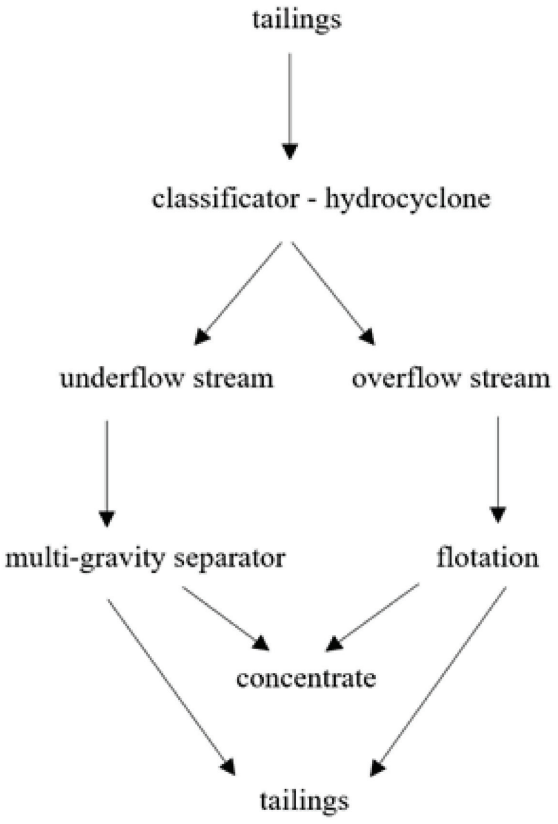

Figure 6: *Process line for copper tailings reprocessing.*

d: ratio of oxidised to intact tailings
e: efficiency of copper reprocessing (share of copper recovered from tailings)
f: share of tailinrgs not yet reprocessed

Given the current world copper demand (about 20 million tons per year), this potential corresponds to the same amount of copper produced from the deposits in about three years.

Conclusions

Despite the fact that the extraction and use of copper has a very long history, most copper has been mined in the 20th and 21st centuries. Copper consumption is increasing over the years, and the price of this commodity is growing accordingly. The extraction of copper accumulated in tailings dams around the world will be an increasing part of the mosaic of copper supply in the future.

At today's copper prices and processing technologies, reprocessing old copper tailings is generally economically viable and cheaper than recovering copper from deposits. Reprocessing tailings can withstand a slightly lower copper content, as there are no costs of excavation, crushing, or grinding.

Tests on samples of tailings have proved the usefulness of MGS in the reprocessing of copper tailings. However, MGS alone cannot provide sufficient recovery such that a concentrate could be prepared directly for smelting; instead, it must be combined with another process such as flotation.

The reprocessing of tailings not only brings additional amounts of copper into the supply chain, but also benefits the environment because the accumulated heavy metals burden the environment. Only copper reprocessing is discussed in this paper. Other metals are also accumulated within tailings dams in larger quantities and can be recovered profitably, which would also benefit the environment.

Acknowledgements

I would like to thank assistant Blaž Janc for helping me with the pictures.

References

[1] 'Copper – A Metal for the Ages', *U.S. Geological Survey, Mineral Resources Program*, https://pubs.usgs.gov/fs/2009/3031/FS2009-3031.pdf., pp.1-4, (accessed 24 May 2021).
[2] McHenry, C. (ed.), *The New Encyclopedia Britannica 3*, 15 edn., Chicago, Encyclopedia Britannica, Inc., 1992, pp.308-310.
[3] 'Copper Prices Hit Highest Level Since 2011' , *Eurometal*, https://eurometal.net/copper-prices-hit-highest-level-since-2011/, (accessed 22 May 2021).
[4] 'LME Copper Historical Price Graph', *London Metal Exchange*, https://www.lme.com/en-GB/Metals/Non-ferrous/Copper#tabIndex=2, (accessed 24 May 2021).
[5] 'Total Copper Mine Production Worldwide from 2006 to 2020', *Statista*, *https://www.statista.com/*

statistics/254839/copper-production-by-country/, (accessed 26 May 2021).

[6] 'World Production Trend of Copper', *U.S. Geological Survey*, https://commons.wikimedia.org/wiki/File:Copper_-_world_production_trend.svg. (accessed 26 May 2021.)

[7] Mackay, I. et al., 'Dynamic Froth Stability of Copper Flotation Tailings', *Minerals Engineering*, no. 124, DOI:10.1016/j.mineng.2018.05.0052018, pp. 103–107.

[8] Drobe, M. et al., 'Processing Tests, Adjusted Cost Models and the Economies of Reprocessing Copper Mine Tailings in Chile', *Metals*, vol. 11, no. 1, 2021, p. 103, DOI:10.3390/met11010103, (accessed 26 May 2021).

[9] Figueiredo, J. et al., 'Tailings Reprocessing from Cabeço do Pião Dam in Central Portugal: A Kinetic Approach of Experimental Data', *Journal of Sustainable Mining*, no. 17, 2018, pp. 139–144, DOI:10.1016/j.jsm.2018.07.001, (accessed 28 May 2021).

[10] Wills, B.A., Finch, J.A., *Wills' Mineral Processing Technology: An Introduction to the Practical Aspects of Ore Treatment and Mineral Recovery,* 8th edn. Oxford, Butterworth-Heinemann, 2016, pp. 1-23, DOI:10.1016/B978-0-08097053-0.00012-1 (accessed 27 May 2021).

[11] 'Processes: Copper Mining and Production', *European Copper Institute*, https://copperalliance.eu/about-copper/copper-and-its-alloys/processes/, pp. 1-3, (accessed 25 May 2021).

[12] Wirth, P., Černič Mali, B., Fischer, W., *Post-Mining Regions in Central Europe – Problems, Potentials,* Possibilities, Munich, Oekom Verlag, 2012, pp. 104-118.

[13] Uekoetter, F., *Mining in Central Europe – Perspectives from Environmental History, Munich, RCC Perspectives,* 2012, DOI:10.5282/rcc/5600, pp. 21-38, (accessed 28 May 2021).

[14] Kastivnik J., Venta A., *Report on Processing Test*, Ljubljana, Geološki Zavod, 2018, pp. 4-17.

[15] Stražišar, J., *Mehanska Procesna Tehnika I.* Ljubljana, Univerza v Ljubljani, 1996, pp. 27-30.

[16] Stražišar, J., Knez, S., *Vaje in Računski Primeri Iz Mehanske Procesne Tehnike*, Ljubljana Univerza v Ljubljani:, 2001, pp. 23-29.

[17] Enhanced Gravity Separator 911mpe-c-902, *911 Metalurgy Coporation*, https://www.911metallurgist.com/equipment/enhanced-gravity-separator/, pp. 1-20. (accessed 11 June 2021).

[18] Rao, G.V., Markandeya, R., Kumar, R. 'Modeling and Optimization of Multi Gravity Separator for Recovery of Iron Values from Sub Grade Iron Ore Using Three Level Three Factor Box Behnken Design', *International Journal of Mineral Processing and Extractive Metallurgy,* no. 2, 2017, pp. 46–56, DOI:10.11648/j.ijmpem.20170204.12. (accessed 28 May 2021).

Original Scientific Article • DOI: 10.2478/rmzmag-2021-0003

Received: July 12, 2021
Accepted: July 15, 2021

Regression methods for evaluation of the underwater noise levels in the Slovenian Sea

Korelacijske in regresijske metode za ocenjevanje ravni podvodnega hrupa

Andreja Popit*
Institute for Water of the Republic of Slovenia
*Corresponding author: E-mail: andreja.popit@izvrs.si

Abstract in English

Anthropogenic underwater noise pollution of seas and oceans caused by shipping can have negative effects on marine animals. The aim of this study was to evaluate quantitatively how much the underwater noise levels in the Slovenian Sea were influenced by anthropogenic pressures and meteorological parameters in the period from 2015 until 2018. For this purpose, correlation method and least squares multiple linear regression analysis were used. The results of this study show that the correlation of underwater noise levels with the dredging activity is significant but low, while correlation with the ship densities is insignificant, which could be due to reduced sound wave propagation in the shallow sea levels. Correlation of the underwater noise levels with the wind speed was significant but low to medium, which could be explained by the breaking waves generated by the wind that produced sound.

Keywords: Underwater noise, correlation, multiple linear regression, anthropogenic pressures, meteorological parameters

Abstract in Slovene

Antropogeno onesnaževanje morij in oceanov s podvodnim hrupom zaradi ladijskega prometa ima lahko negativen vpliv na morske živali. Cilj te študije je bil kvantitativno oceniti, koliko so bile vrednosti ravni podvodnega hrupa v slovenskem morju odvisne od antropogenih pritiskov in meteoroloških parametrov v obdobju od 2015 do 2018. V ta namen sta bili uporabljeni korelacijska metoda in multipla linearna regresijska analiza z metodo najmanjših kvadratov. Rezultati te študije so pokazali, da je bila korelacija ravni podvodnega hrupa z aktivnostjo poglabljanja morskega dna signifikantna, toda nizka, medtem ko je bila korelacija z gostoto ladij zanemarljiva, kar je lahko posledica zmanjšanega širjenja zvočnega valovanja v plitvem morju. Korelacija ravni podvodnega hrupa s hitrostjo vetra je bila signifikantna, vendar nizka do srednja, kar je mogoče razložiti z zvokom nastalim zaradi lomljenja valov, ki jih je generiral veter.

Ključne besede: Podvodni hrup, korelacija, multipla linearna regresija, antropogeni pritiski, meteorološki parametri

Introduction

Anthropogenic noise pollution is present in a number of world's the seas and oceans, caused, in particular, by marine traffic. Continuous underwater noise from ships disturbs communication of marine mammals, such as dolphins and whales, which causes problems in their orientation, mating, and feeding that are critical to their survival [1, 2].

To study the correlations of underwater noise with ship traffic that is representative for shallow waters worldwide, examples were chosen in the Celtic and North Seas of the UK, the Scotian Shelf of Canada, the Guanabara Bay in Southeast Brazil and in the shallow waters of the Indian Ocean. An example of the underwater noise of biological origin was chosen in the lagoon of a coral atoll in the Indian Ocean. For correlations of underwater noise with the

ship traffic representative of deep waters examples were chosen in the Northeast Pacific Ocean in the USA; the Ramsey Sound, Pembrokeshire, West Wales in the UK; and the Gulf of Mexico (Table 1).

An analysis of shallow-water ambient noise levels collected during 14 cruises was reported for the Scotian Shelf on the eastern Canadian coast over the period from 1972 to 1985 [3]. The frequency range covered was 30 Hz to 900 Hz. It was found that the average ambient noise levels (Table 1) were characteristic of shallow water areas with high shipping densities.

The results of an analysis of temporal fluctuations in the noise power spectrum level of shallow water ambient noise in the bandwidth of 100 Hz to 4 kHz were presented in India [4]. The results showed that variation in the average noise spectrum level was higher in the lower frequency level (100 Hz to 1 kHz) (Table 1) and assumed a constant level from there onwards. It was concluded that the temporal fluctuations of the noise levels were due mostly to ship traffic and changes in the weather conditions [4].

Frequency spectra of the underwater ambient noise were measured in the lagoon of a coral atoll, outside the reef and on shallow-water banks in the tropical zone of the Indian Ocean [5]. The measurements were performed in the frequency range of 0.003–9 kHz. In all the regions studied, continuous underwater noise (Table 1) of biological origin was observed, attributed to croaker fish [5].

Continuous measurements of underwater noise levels in the Northeast Pacific Ocean west of San Nicolas Island, California, USA over 138 days, spanning 2003–2004 were compared with measurements made during the 1960s at the same site (Table 1) [6]. Ambient noise levels at 30–50 Hz were 10–12 dB higher in 2003–2004 than in 1964–1966 (Table 1), suggesting an average noise increase rate of 2.5–3 dB per decade. Low frequency (10–50 Hz) ocean ambient noise levels were closely related to the shipping vessel traffic. Increases in commercial shipping were believed to account for the observed low-frequency ambient noise increase. Above 50 Hz the noise level differences between recording periods gradually diminished to only 1–3 dB at 100–300 Hz [6].

Higher underwater noise levels were measured in the area of Ramsey Sound, Pembrokeshire, West Wales, UK, in the summer of 2009 during the season with increased boat traffic (Table 1) compared with the underwater noise levels measured in the spring of 2009 during the season with decreased boat traffic [7]. Below 2 kHz, the noise was thought to come from boat traffic. The peak in sound pressure level around 10 Hz in both seasons was thought to originate from a variety of shipping-related sources, including propeller-excited hull resonance, hull pressure, or propeller blades which could appear from 4 to 70 Hz. These lower frequencies could originate from surface noise due to waves associated with shipping or from breaking on the rocks. The survey taken in the summer, during periods of increased tourist boat activity, showed a distinct peak around 100 Hz that was not apparent during the low season survey. The origin of this noise was likely to be diesel engines, propeller cavitation, engine harmonics and gearboxes [7].

The first study in Brazil to characterise noise levels in the coastal zone was carried out in Guanabara Bay (Southeast Brazil). It showed underwater noise pollution related to the ship traffic and small vessel traffic (Table 1) [8]. Locations with ship traffic had the highest noise levels, while locations with small vessel traffic had the lowest noise levels.

Elevated noise conditions were observed across the Gulf of Mexico, where anthropogenic marine activities were prominent [9]. The LF (low frequency) band was selected to include the environmental, meteorological, biological, and anthropogenic sounds that occur primarily between 10 Hz and 500 Hz. At recording sites positioned nearest to high-density shipping lanes that lead to the Port of South Louisiana (H-3) and the Port of Houston (H-1) the highest L_{01} values (T = 1 h) were recorded (Table 1) [9].

Nationally coordinated efforts to quantify underwater noise levels in the UK were presented, in support of UK policy objectives under the EU Marine Strategy Framework Directive (MSFD) [10]. Field measurements were made during 2013 and 2014 at twelve sites around the UK (Table 1). Noise exposure varied considerably, with little anthropogenic influence

Table 1: *Examples of underwater noise levels related mainly to the ship traffic in the global seas and oceans.*

Location, depth of the hydrophone and depth of the sea water	Year of study	Underwater noise levels at different frequencies	Location, depth of the hydrophone and depth of the sea water	Year of study	Underwater noise levels at different frequencies
Scotian Shelf, Canada, hydrophone depth of 31 m and water depth of 79 m [3]	1972–1985	Winter average noise levels at zero wind speed [3]: 30 Hz: 90.8 dB re μPa²/Hz 45 Hz: 90.5 dB re μPa²/Hz 80 Hz: 87.9 dB re μPa²/Hz 150 Hz: 81.9 dB re μPa²/Hz 300 Hz: 74.1 dB re μPa²/Hz 600 Hz: 64.4 dB re μPa²/Hz 900 Hz: 64.3 dB re μPa²/Hz	Ramsey Sound, Pembrokeshire, West Wales, UK, hydrophone depth of 20 m and a water depth of 460 m [7]	2009	Sound pressure levels [7]: Between 5 Hz and 10 Hz: - 92.6 dB re 1 μPa ± 3.9 dB re 1 μPa during spring - 104.7 dB re 1 μPa ± 2.2 dB re 1 μPa during summer Around 100 Hz: - 85.9 dB re 1 μPa ± 2.4 dB re 1 μPa during spring - 104.6 dB re 1 μPa ± 2.4dB re 1 μPa during summer
India, shallow water, hydrophone depth of 5 m and water depth of 25 m [4]	2006	Average noise levels [4]: 98 Hz: 130.3 dB re μPa/√Hz 195 Hz: 128.6 dB re μPa/√Hz 293 Hz: 127.3 dB re μPa/√Hz 586 Hz: 127.6 dB re μPa/√Hz 977 Hz: 127.4 dB re μPa/√Hz 3027 Hz: 127.1 dB re μPa/√Hz 4023 Hz: 127.1 dB re μPa/√Hz	Guanabara Bay, SE Brazil, hydrophone depth of 2 m and a water depth of 4 m [8]	2011–2012	The highest mean sound pressure level [8]): At 187 Hz: 111.6 ± 9.0 dB re 1 μPa At 15.89 kHz: 76.2 ± 8.3 dB re 1 μPa
Indian Ocean, the lagoon of a coral atoll, hydrophone depth of 2–15 m and water depth of 50 m [5]	2005	Spectral maxima observed at 1 kHz and 7.5 kHz [5]: 1,000 Hz: 72 dB re μPa/√Hz 2,000 Hz: 65 dB re μPa/√Hz 7,500 Hz: 80 dB re μPa/√Hz	Port of South Louisiana (H-3), Port of Houston (H-1), NE Gulf of Mexico, hydrophone depth from 250–1,370 m [9]	2010–2012	The highest values L_{01} (T = 1 h) at two sites (H-3 and H-1) nearest to high-shipping lanes [9] in LF band (10–500 Hz) were: 130 dB re 1 μPa and 128 dB re 1 μPa, respectively (L_{01} = sound levels that were exceeded 1% of the time)
Northeast Pacific Ocean, SW of the San Nicolas Island, California, USA, hydrophone depth of 1,090–1,106 m [6]	1966 – 2006	Mean ambient noise levels: -30–50 Hz in 1964–1966: 73–75 dB re 1 Pa²/Hz -30–50 Hz in 2003–2004: 85 dB re 1 Pa²/Hz [6]	Celtic Sea, northern and southern North Sea in UK, hydrophone depth of 100 m and a water depth of 200 m [10]	2013– 2014	Median noise levels for 1/3 octave bands from 63 Hz to 500 Hz [10]: 81.5–95.5 dB re 1μPa

at the Celtic Sea site to several North Sea sites with persistent vessel noise [10].

The above studies showed that man-made noise pollution is present in a number of world seas and oceans caused, in particular, by the maritime traffic (Table 1).

In January 2019, a group of NGOs specialising in the protection of marine life warned that most EU member states were probably not going to honour their commitment to reduce marine noise pollution by 2020 [11]. In this regard, methodological guidance on the underwater noise mitigation measures were prepared by ACCOBAMS in 2019 [12]. These are very useful to be taken into consideration in order to successfully mitigate underwater noise sources in the worlds' seas and oceans.

The aim of this study was to prepare a methodology for quantitative determination of the relationship of the measured underwater noise levels in the Slovenian Sea with anthropogenic pressures and meteorological parameters.

The content of the study is important primarily from the point of view of properly recognising the correlation between the pressures and the status of the marine environment and of determining the optimal mitigating measures for achieving the objective of the Marine Directive (2008/56/EC) [13].

Materials and methods

Underwater noise is monitored near the lighthouse foundation 300 m off the coast at Debeli rtič, Slovenia (lat.: 45°35' 28.2'' N, lon.: 13°41' 59.1'' E), beginning in February 2015. Hydrophone of type Bruel and Kjaer 8,105 was installed 1 m away from the lighthouse foundation at a depth of 4 m (sea depth is 5 m) and connected to a sound analyser of type Bruel and Kjaer 2,250, with a sound level meter and an octave-based frequency analyser that operates in the frequency range of 6.3 Hz to 20 kHz [14]. A sound analyser is closed inside the lighthouse. Measuring unit of the underwater noise levels is dB re µPa.

Dependent variables were continuous underwater noise levels (in dB) in 1/3 octave bands with center frequencies of 63 Hz and 125 Hz, $L_{eq,63Hz}$ and $L_{eq,125Hz}$ (dB). Independent variables were ship densities in the four different areas of 2 NM and 5 NM from the measuring station, in the Gulf of Trieste and in the Gulf of Venice ($\rho_{L,2\ NM}$, $\rho_{L,\ 5NM}$, $\rho_{L,Trieste}$, $\rho_{L,Venice}$), dredging activities, cleaning of the sea floor, wind speed at v_v (m/s) and precipitation at h_p (mm). Wind speed data from the Piran buoy and precipitation data from the meteorological station in the Port of Koper were obtained from the Environmental Agency of the Republic of Slovenia. Ship densities were provided from Automatic Information System data [15].

Measuring periods were the following: from 13 February 2015 to 5 May 2015; from 26 September 2015 to 31 December 2015; from 18 August 2016 to 1 November 2016; from 6 July 2017 to 27 August 2017; and from 18 August 2018 to 31 December 2018, in which measured underwater noise levels were available.

For the analysis of the correlation between the dependent variables and the independent variables, the Pearson correlation coefficient *r* was used [16], which is a measure of the linear correlation between the two variables that gives information about the degree, or magnitude, of the association or correlation, as well as of the direction (+/-) of the relationship between the variables. It is most suitable for use if the distribution of variables is normal (or at least symmetric and unimodal). With *r* we can examine whether two variables tend to move together. If the large values of one variable are related to the large values of the other variable, the correlation is positive. If the small values of one variable are related to the large values of the other variable, the correlation is negative. If the values of the two variables are not related, the correlation is close to or equal to 0.

The results of the analysis of the correlation between dependent and independent variables are presented in tables, the results being interpreted and the weights of the influence of the anthropogenic and meteorological noise sources on the measured underwater noise levels estimated.

With this correlation analysis, the interdependence of dependent and independent variables was investigated, while multiple linear

regression analysis was used to study how strongly the values of the dependent variables were affected by the values of independent variables. To predict the dependent variables from independent variables, a linear regression model was used, including the least squares method, in which the sum of the squares of deviations is minimal.

The multiple correlation coefficient r between the dependent variables and the independent variables was analysed, and the results are presented in the next section.

The quality of the regression model was evaluated based on the coefficient of determination R^2, which tells how much of the variance of the dependent variables is explained by the variability of the independent variable – ie explained variance. In the case of the linear regression, it is equal to the square of the Pearson correlation coefficient, R^2. However, 1 - R^2 is an unexplained variance and its root is a standard prediction error.

The test of statistical significance of the correlation was performed based on p-values (significance level). In the regression equation, those variables that have a p-value of less than 0.05 are significant, which means that there is less than a 5 % probability that the correlation is due to an error, which means that there is a 95 % probability that the variables are related to each other.

If the p-value is less than or equal to 0.05 ($p \leq 0.05$), then the results can be generalised with high certainty (95%) from the sample to the population, ie that there are differences between the two variables or that the two variables are interrelated. If the p-value is greater than 0.05 ($p > 0.05$), then the results cannot be generalised from the sample to the population, and we must interpret the results only at the sample level.

From the regression analysis, we estimated the weights of the influence of the anthropogenic and meteorological noise sources on the levels of underwater noise measured.

Results and discussion

The average $L_{eq,63\text{Hz}}$ and $L_{eq,125\text{Hz}}$ levels measured in the Slovenian Sea in the period between 2015 and 2018 were 82.8–101.1 dB re 1 µPa and 83.9–98.1 dB re 1 µPa, respectively. The average ship densities were 2–252. The average wind speed was 1.8–4.6 m/s and the average precipitation was 0.02–0.07 mm [14].

Results of the correlation analysis

Interdependence between the dependent ($L_{eq,63Hz}$ and $L_{eq,125Hz}$) and independent ($\rho_{L,2NM}$, $\rho_{L,5NM}$, $\rho_{L,Trieste}$, $\rho_{L,Venice}$, dreadg. act., clean. act., v_v and h_p) variables using the Pearson correlation coefficients is presented in Table 2 (for $L_{eq,63Hz}$) and Table 3 (for $L_{eq,125Hz}$).

The highest correlation between the underwater noise and the anthropogenic noise sources was obtained between the $L_{eq,63\text{Hz}}$ and the dredging activities ($r = 0.31$) (Table 2). The highest correlation between the underwater noise

Table 2. *The Pearson correlation coefficients between the dependent variable ($L_{eq,63Hz}$) and the independent variables ($\rho_{L,2NM}$, $\rho_{L,5NM}$, $\rho_{L,Trieste}$, $\rho_{L,Venice,}$ dreadg. act., clean. act., v_v and h_p) in all measuring periods.*

Pearson's correlation coefficient	From 13.02.2015 to 05.05.2015	From 26.09.2015 to 31.12.2015	From 18.08.2016 to 01.11.2016	From 06.07.2017 to 07.08.2017	From 18.08.2018 to 31.12.2018
r (v_v)	0.58	0.51	0.54	0.39	0.35
r (h_p)	-0.02	0.06	0.08	0.08	0.07
r ($\rho_{L,2\text{NM}}$)	0.13	-0.06	0.05	-0.04	0.05
r ($\rho_{L,5\text{NM}}$)	0.06	-0.06	0.02	0.09	0.08
r ($\rho_{L,\text{Trieste}}$)	-0.02	-0.03	0.08	0.12	0.12
r ($\rho_{L,\text{Venice}}$)	-0.10	-0.05	-0.05	0.01	-0.11
r (dredg. act.)	n.a.	0.31	n.a.	n.a.	n.a.
r (clean. act.)	n.a.	n.a.	-0.10	n.a.	n.a.

Table 3: *The Pearson correlation coefficients between the dependent variable ($L_{eq,125Hz}$) and the independent variables ($\rho_{L,2NM}$, $\rho_{L,5NM}$, $\rho_{L,Trieste}$, $\rho_{L,Venice,}$ dreadg. act., clean. act., v_v and h_p) in all measuring periods.*

Pearsons correlation coefficients	From 13.02.2015 to 05.05.2015	From 26.09.2015 to 31.12.2015	From 18.08.2016 to 01.11.2016	From 06.07.2017 to 07.08.2017	From 18.08.2018 to 31.12.2018
r (v_v)	0.39	0.18	0.55	0.24	0.15
r (h_p)	-0.02	0.01	0.09	0.04	0.02
r ($\rho_{L,2NM}$)	0.11	0.06	0.07	0.02	0.12
r ($\rho_{L,5NM}$)	0.05	0.05	-0.04	0.17	0.02
r ($\rho_{L,Trieste}$)	-0.02	0.02	0.01	0.18	0.04
r ($\rho_{L,Venice}$)	-0.08	-0.01	-0.09	-0.01	-0.10
r (dredg. act.)	n.a.	0.10	n.a.	n.a.	n.a.
r (clean. act.)	n.a.	n.a.	-0.10	n.a.	n.a.

($L_{eq,63Hz}$ and $L_{eq,125Hz}$) and the ship density ($\rho_{L,2NM}$, $\rho_{L,5NM}$, $\rho_{L,Trieste}$, $\rho_{L,Venice}$) was 0.18. Correlation between the underwater noise ($L_{eq,63Hz}$ and $L_{eq,125Hz}$) and the cleaning of the sea floor was -0.10.

Correlation analyses showed that the relationship between the $L_{eq,63Hz}$ and the v_v was between 0.35 and 0.58, while that between $L_{eq,125Hz}$ and the $v_{v,}$ was between 0.15 and 0.55. The relation between the underwater noise ($L_{eq,63Hz}$ and $L_{eq,125Hz}$) and the meteorological parameter – precipitation, h_p – was between -0.02 and 0.09 (Tables 2 and 3). These results of the correlation analyses are interpreted in the subsection discussion.

Results of the multiple linear regression analysis

Furthermore, the least squares multiple linear regression analysis in Table 4 shows how much the values of the dependent variables were affected by the values of the independent variables. The multiple correlation coefficients between the dependent variable $L_{eq,63Hz}$ and the independent variables in all measuring periods were moderate (r = 0.40 – 0.59), while those between the dependent variable $L_{eq,125Hz}$ and the independent variables were low to moderate (r = 0.21 – 0.59) (Table 4).

In the regression analysis, 16%–35% of the variance of the dependent variable $L_{eq,63Hz}$ and 5%–34% of the variance of the dependent variable $L_{eq,125Hz}$ can be explained by the variability of the independent variables ($\rho_{L,2NM}$, $\rho_{L,5NM}$, $\rho_{L,Trieste}$, $\rho_{L,Venice}$, *dreadg. act., clean. act., vv and hp*), with which the predictive power of the multiple regression model is shown (Table 5).

The statistical significance test of the correlation based on the p-value indicated that there was only one independent variable, wind speed vv, that had a significant correlation with both dependent variables ($L_{eq,63Hz}$ and $L_{eq,125Hz}$) in all the measuring periods (Tables 6 and 7). Dredging and cleaning activities also had a significant correlation with $L_{eq,63Hz}$ *and* $L_{eq,125Hz}$. Precipitation, hp, was mostly insignificant. Ship densities ($\rho_{L,2NM}$, $\rho_{L,5NM}$, $\rho_{L,}$*Trieste,* $\rho_{L,}$*Venice*) were in some cases significant and in some insignificant.

Subsequently, the multiple regression analysis was repeated without the insignificant independent variables in each measuring period. Regression equations in which the dependent variables ($L_{eq,63Hz}$ and $L_{eq,125Hz}$) were predicted by the significant independent variables are presented in Tables 8 and 9.

Discussion of the results

The average continuous underwater noise levels ($L_{eq,63Hz}$ and $L_{eq,125Hz}$) measured in the Slovenian Sea [13] were similar to those reported in the literature, which were related to the shipping noise (Table 1).

Multiple correlation coefficients between the dependent variables ($L_{eq,63Hz}$ and $L_{eq,125Hz}$)

Table 4: *Multiple correlation coefficients (r) between dependent variables ($L_{eq,63Hz}$ and $L_{eq,125Hz}$) and independent variables ($\rho_{L,2NM}$, $\rho_{L,5NM}$, $\rho_{L,Trieste}$, $\rho_{L,Venice,}$ dreadg. act., clean. act., v_v and h_p) in all measuring periods.*

Multiple correlation coefficients	From 13.02.2015 to 05.05.2015	From 26.09.2015 to 31.12.2015	From 18.08.2016 to 01.11.2016	From 06.07.2017 to 07.08.2017	From 18.08.2018 to 31.12.2018
$r\ (L_{eq,63Hz})$	0.59	0.55	0.57	0.40	0.40
$r\ (L_{eq,125Hz})$	0.41	0.21	0.59	0.29	0.23

Table 5: *Coefficients of determination (R^2) between the dependent variables ($L_{eq,63Hz}$ and $L_{eq,125Hz}$) and the independent variables ($\rho_{L,2NM}$, $\rho_{L,5NM}$, $\rho_{L,Trieste}$, $\rho_{L,Venice,}$ dreadg. act., clean. act., v_v and h_p) in all measuring periods.*

Coefficients of determination	From 13.02.2015 to 05.05.2015	From 26.09.2015 to 31.12.2015	From 18.08.2016 to 01.11.2016	From 06.07.2017 to 07.08.2017	From 18.08.2018 to 31.12.2018
$R^2\ (L_{eq,63Hz})$	0.35	0.30	0.33	0.16	0.16
$R^2\ (L_{eq,125Hz})$	0.17	0.05	0.34	0.09	0.05

Table 6: *Significant independent variables with p-values lower than 0.05, meaning that there was a more than 95 % probability that these variables were related to the dependent variable $L_{eq,63Hz}$. The grey fields indicate insignificant independent variables, with p-values greater than 0.05. The abbreviation n.a. means not applicable.*

p-values	From 13.02.2015 to 05.05.2015	From 26.09.2015 to 31.12.2015	From 18.08.2016 to 01.11.2016	From 06.07.2017 to 07.08.2017	From 18.08.2018 to 31.12.2018
$p\ (v_v)$	0.000	0.000	0.000	0.000	0.000
$p\ (h_p)$	0.001	0.061	0.240	0.923	0.010
$p\ (\rho_{L,2NM})$	0.005	0.691	0.048	0.003	0.036
$p\ (\rho_{L,5NM})$	0.007	0.015	0.000	0.556	0.000
$p\ (\rho_{L,Trieste})$	0.327	0.794	0.000	0.119	0.000
$p\ (\rho_{L,Venice})$	0.037	0.087	0.023	0.342	0.000
p (dredg. act.)	n.a.	0.000	n.a.	n.a.	n.a.
p (clean. act.)	n.a.	n.a.	0.002	n.a.	n.a.

Table 7: *Significant independent variables with p-values less than 0.05, meaning that there was a more than 95 % probability that these variables were related to the dependent variable $L_{eq,125Hz}$. The grey fields indicate insignificant independent variables with p-values greater than 0.05. The abbreviation n.a. means not applicable.*

p-values	From 13.02.2015 to 05.05.2015	From 26.09.2015 to 31.12.2015	From 18.08.2016 to 01.11.2016	From 06.07.2017 to 07.08.2017	From 18.08.2018 to 31.12.2018
$p\ (v_v)$	0.000	0.000	0.000	0.000	0.000
$p\ (h_p)$	0.019	0.509	0.111	0.867	0.599
$p\ (\rho_{L,2NM})$	0.097	0.022	0.000	0.033	0.000
$p\ (\rho_{L,5NM})$	0.000	0.000	0.000	0.215	0.002
$p\ (\rho_{L,Tireste})$	0.001	0.000	0.000	0.033	0.000
$p\ (\rho_{L,Venice})$	0.256	0.110	0.036	0.000	0.000
p (dredg. act.)	n.a.	0.000	n.a.	n.a.	n.a.
p (clean. act.)	n.a.	n.a.	0.021	n.a.	n.a.

Table 8: *Regression equations in which the dependent variable $L_{eq,63Hz}$ was predicted by the significant independent variables ($\rho_{L,2NM}$, $\rho_{L,5NM}$, $\rho_{L,Trieste}$, $\rho_{L,Venice,}$ dreadg. act., clean. act., v_v and h_p).*

Measuring periods	Regression equations
13.02.2015–05.05.2015	$L_{eq,63Hz} = 1.378*v_v - 3.898*h_p + 0.357*\rho_{L,2NM} + 0.103*\rho_{L,5NM} - 0.014*\rho_{L,Venice} + 63.450$
26.09.2015–31.12.2015	$L_{eq,63Hz} = 1.117*v_v - 0.093*\rho_{L,5NM} + 4.304*$dred.act. $+ 67.800$
18.08.2016–01.11.2016	$L_{eq,63Hz} = 2.227*v_v + 0.165*\rho_{L,2NM} - 0.627*\rho_{L,5NM} + 0.528*\rho_{L,Trieste} - 0.012*\rho_{L,Venice} - 3.1*$clean.a. $+ 81.77$
06.07.2017–07.08.2017	$L_{eq,63Hz} = 2.762*v_v - 0.196*\rho_{L,2NM} + 70.065$
18.08.2018–31.12.2018	$L_{eq,63Hz} = 1.555*v_v + 1.116*h_p + 0.112*\rho_{L,2NM} - 0.216*\rho_{L,5NM} + 0.268*\rho_{L,Trieste} - 0.022*\rho_{L,Venice} + 73.576$

Table 9: *Regression equations in which the dependent variable $L_{eq,125Hz}$ was predicted by the significant independent variables ($\rho_{L,2NM}$, $\rho_{L,5NM}$, $\rho_{L,Trieste}$, $\rho_{L,Venice,}$ dreadg. act., clean. act., v_v and h_p).*

Measuring periods	Regression equations
13.02.2015–05.05.2015	$L_{eq,125Hz} = 0.752*v_v - 2.659*h_p + 0.263*\rho_{L,5NM} - 0.153*\rho_{L,Trieste} + 77.786$
26.09.2015–31.12.2015	$L_{eq,125Hz} = 0.248*v_v + 0.192*\rho_{L,2NM} + 0.167*\rho_{L,5NM} - 0.117*\rho_{L,Trieste} + 1.181*$dred. $+ 77.375$
18.08.2016–01.11.2016	$L_{eq,125Hz} = 1.869*v_v + 0.265*\rho_{L,2NM} - 0.551*\rho_{L,5NM} + 0.368*\rho_{L,Trieste} - 0.009*\rho_{L,Venice} - 1.87*$ clean.a. $+ 84.6$
06.07.2017–07.08.2017	$L_{eq,125Hz} = 1.063*v_v - 0.122*\rho_{L,2NM} + 0.151*\rho_{L,Triestre} - 0.017*\rho_{L,Venice} + 71.912$
18.08.2018–31.12.2018	$L_{eq,125Hz} = 0.562*v_v + 0.364*\rho_{L,2NM} - 0.126*\rho_{L,5NM} + 0.121*\rho_{L,Trieste} - 0.017*\rho_{L,Venice} + 91.705$

and independent variables (anthropogenic pressures and meteorological parameters) were low to moderate (r = 0.21 – 0.59) (Table 4). In the regression analysis up to 35 % of the variance of the dependent variable can be explained by the independent variables (Table 5).

The correlation coefficient between the measured underwater noise levels ($L_{eq,63Hz}$) and dredging activity as an anthropogenic noise source was significant but low (r = 0.31) (Table 2). The highest correlation between the underwater noise levels ($L_{eq,63Hz}$ and $L_{eq,125Hz}$) and the ship densities was up to 0.13 and 0.18, respectively (Tables 2 and 3), which could be explained by reduced sound wave propagation in the shallow sea [10,17–19]. Low frequency sound waves below the cut-off frequency do not propagate, because the sound propagates into the sea bed [20, 21]. The correlation between underwater noise and the cleaning of the sea floor was negligible (Tables 2 and 3), which was expected, because cleaning was performed with an excavator from the mainland.

The relation between underwater noise and the meteorological parameter – precipitation – was insignificant. Correlation between the $L_{eq,63Hz}$ and the wind speed was low to medium and correlation between the $L_{eq,125Hz}$ and the wind speed was negligible to medium (Tables 2 and 3), which could be explained by the wind-generated waves that break when they are large enough and produce sound [22–28]. That is, underwater ambient sound measurements were, in some cases, used to estimate wind speed over the seas and oceans. The results of these cases showed a very strong correlation between estimated wind speed, provided by a passive acoustic recorder algorithm and in situ measurements of the wind speed [29, 30].

Relevant to our study is the problem of selection of frequencies in the 1/3 octave band as indicators of shipping noise. We based our measurements on the European Marine

Strategy Framework Directive which focuses on low frequency vessel noise, in 1/3 octave bands with centre frequencies of 63 Hz and 125 Hz, as pressure indicators for ship noise [31]. The two bands were selected based on recordings of ship noise in deep-water areas where, in general, these bands are most powerful [22]. A Danish study of ship noise in shallow water has shown that the aforementioned MSFD indicators of shipping noise turned out to be poor proxies for the impact of noise on small cetaceans at higher frequencies. Thus, higher frequencies were proposed to be included in the assessment of good environmental status, ie in the 1/3 octave band with a centre frequency of 10 kHz, which was chosen as a compromise between the range of hearing of small cetaceans and frequency dependent absorption [32]. For this reason, higher frequencies should also be included in further studies of underwater noise in the northern, shallow part of the Adriatic Sea.

Conclusions

Given the multiple linear regression analysis we conclude that dependent variables were affected by the values of independent variables to a low to moderate degree. The correlation of the underwater noise levels with the dredging activity was significant but low, and the one with the ship densities was insignificant, which could be explained by reduced sound wave propagation in the shallow sea. The correlation between underwater noise and the cleaning of the sea floor was negligible, which could be explained by the fact that cleaning was performed with an excavator from the mainland. The relation between the underwater noise and the meteorological parameter – precipitation was insignificant, while correlation between underwater noise and the wind speed was significant but low to medium, which could be explained by the breaking waves generated by the wind that produced sound.

In the near future, the methodology presented will be used to evaluate underwater noise data measured in the years 2019 and 2020. In addition to MSFD pressure indicators for ship noise in 1/3 octave bands with center frequencies of 63 Hz and 125 Hz higher frequencies will be included.

Acknowledgements

This research was funded by the Slovenian Ministry for the Environment and Spatial Planning. AIS data for the year 2015 were obtained during implementation of the European project BALMAS (2013–2016) from the Italian Coast Guard Headquarters, who gave us permission to use the AIS data for our analyses. AIS data from 2016 to 2018 were obtained by the Slovenian Maritime Administration in the frame of the Ministry for Infrastructure.

References

[1] Southall, B.L. et al., 'Underwater Noise from Large Commercial Ships —International Collaboration for Noise Reduction', *Encyclopedia of Maritime and Offshore Engineering*, (LOCATION OF PUBLISHER?), John Wiley & Sons, 2017 DOI:10.1002/9781118476406.emoe056.

[2] Marley, S.A., Salgado-Kent, C.P., Erbe, C., Parnum, I.M. 'Effects of Vessel Traffic and Underwater Noise on the Movement, Behavior and Vocalizations of Bottlenose Dolphins in an Urbanized Estuary', *Scientific Reports,* vol. 7, no. 13,437, 2017, pp. 1–14, DOI:10.1038/s41598-017-13252-z.

[3] Zakarauskas, P., Chapman, D.M.F., Staal, P.R. 'Underwater Acoustic Ambient Noise Levels on the eastern Canadian continental shelf. *Journal of the Acoustical Society of America*, vol. 87, no. 5, 1990, pp. 2064–2071, DOI:10.1121/1.399333.

[4] Ramji, R., Ramakrishanan, S. 'Analysis of Short Term Temporal Fluctuations in Noise Power Spectrum of Shallow Water Ambient Noise', *Symposium on Underwater Technology and Workshop on Scientific Use of Submarine Cables and Related Technologies*, Tokyo, IEEE, 2007, pp. 113–119.

[5] Bardyshev, V.I. (2007): 'Underwater Ambient Noise in Shallow Water Areas of the Indian Ocean Within the Tropical Zone', *Acoustical Physics*, vol. 53, no. 2, pp. 167–171, DOI:10.1134/S1063771007020091.

[6] McDonald, M.A., Hildebrand, J.A., Wiggins, S.M. 'Increases in Deep Ocean Ambient Noise in the Northeast Pacific West of San Nicolas Island, California', *Journal of the Acoustical Society of America*, no. 120, 2006, pp. 711–718, DOI:10.1121/1.2216565.

[7] Willis, M.R. et al., 'Measuring Underwater Background Noise in High Tidal Flow Environments', *Renewable Energy*, no. 49, 2013, pp. 255–258, DOI:10.1016/j.renene.2012.01.020.

[8] Bittencourt, L. et al., 'Underwater Noise Pollution in a coastal tropical environment', *Marine Pollution Bulletin*, vol. 83, no. 1, 2014, pp. 331–336, DOI:10.1016/j.marpolbul.2014.04.026n.

[9] Estabrook, B.J. et al., 'Widespread Spatial and Temporal Extent of Anthropogenic Noise across the Northeastern Gulf of Mexico Shelf Ecosystem', *Endangered Species Research,* no. 30, 2016 pp. 267–282, DOI:10.3354/esr00743.

[10] Merchant, N.D. et al.,) 'Underwater Noise Levels in UK Waters', *Scientific Reports*, vol. 6, no. 36,942, 2016, (PAGE REF?) DOI:10.1038/srep36942.

[11] European Parliament, 'Parliamentary Questions', https://www.europarl.europa.eu/doceo/document/E-8-2019-001209_EN.html, accessed 15 June 2021.

[12] ACCOBAMS, 'Methodological Guide – Guidance on Underwater Noise Mitigation Measures, Seventh Meeting of the Parties to ACCOBAMS', Istanbul, Republic of Turkey, 2019, p. 31.

[13] Directive of the European Parliament and of the Council (EC/2008/56), 'Establishing a Framework for Community Action in the Field of Marine Environmental Policy (Marine Strategy Framework Directive)', *Official Journal of the European Union*, L164, pp. 19–40.

[14] Popit, A., 'Underwater Noise in the Slovenian Sea', *Materials and Geoenvironment – RMZ,* vol. 67, no. 3, 2020, pp. 1–15, DOI:10.2478/rmzmag-2020-0018.

[15] Perkovič, M., Batista, M., Luin, B., 'Prikaz in Analiza Gostot Ladijskega Prometa', *Fakulteta Za Pomorstvo In Promet*, Lyublyana, Univerza v Ljubljani, 2019, (PAGE REF?)

[16] Davis, J.C., Statistics and Data Analysis in geology. *John Wiley & Sons*, Inc., 1986New York. (PAGE REF?)

[17] Kozaczka, E., Grelowska, G., 'Propagation of Ship-Generated Noise in Shallow Sea', *Polish Maritime Research*, vol. 25, no. 2, 2018, pp. 37–46, DOI:10.2478/pomr-2018-0052.

[18] Meyer, V., Audoly, C.A., 'Comparison Between Experiments and Simulation for Shallow Water Short-Range Acoustic Propagation', *International Congress on Sound and Vibration, ICSV 24th*, London, United Kingdom, 2017. (PAGE REF?)

[19] Duncan, A.J. et al., 'Characteristics of Sound Propagation in Shallow Water over An Elastic Seabed with a Thin Cap-Rock Layer', *Journal of the Acoustical Society of America,* vol. 134, no. 1, 2013, pp. 207–205, DOI:10.1121/1.4809723.

[20] Urick, R.J., *Principles of Underwater Sound*, New York, McGraw-Hill, 1983 (PAGE REF?)

[21] Robinson, S.P., Lepper, P.A. *Scoping Study: Review of Current Knowledge of Underwater Noise Emissions from Wave and Tidal Stream Energy Devices*, London, Crown Estate, 2013, (PAGE REF?)

[22] National Research Council, *Ocean Noise and Marine Mammals*. Washington DC, The National Academies Press, 2003, DOI:10.17226/10564. (PAGE REF?)

[23] Banner, M.L., Cato, D.H. 'Physical Mechanisms of Noise Generation by Breaking Waves – A Laboratory Study', in *Natural Physical Sources of Underwater Sound – Sea Surface Sound*, Kerman, B.R. (ed.), Dordrecht, Kluwer Academic, 1993, pp. 429–436,

[24] Carey, W.M., Fitzgerald, J.W., Browning, D.G., 'Low Frequency Noise Form Breaking Waves', In, *NUSC Technical Report 8783*, New London, Connecticut, Naval Underwater System Center 1990, (PAGE REF?)

[25] Kerman. B.R. 'Underwater Sound Generation by Breaking Wind Waves', *Journal of the Acoustical Society of America*, vol. 75, no. 1, 1984, pp. 149–165, DOI:10.1121/1.390409.

[26] Stewart, M.S., Shallow water ambient noise caused by breaking waves in the surf zone. Ph.D. diss., Naval Postgraduate School, Monterey, California, 1994, (PAGE REF?)

[27] Cuomo, G. et al., 'Breaking Wave Loads at Vertical Seawalls and Breakwaters', *Coastal Engineering*, vol. 57, no. 4, 2010, pp. 424–439, DOI:10.1016/j.coastaleng.2009.11.005.

[28] Ravindar, R., Sriram, V., Schimmels, S., Stagonas, D. 'Characterization of Breaking Wave Impact on Vertical Wall with Recurve', *ISH Journal of Hydraulic Engineering*, vol. 25, no. 2, 2019, pp. 153–161, DOI:10.1080/09715010.2017.1391132.

[29] Vagle, S., Large, W.G., Farmer, D.M. An Evaluation of the WOTAN Technique of Inferring Oceanic Winds from Underwater Ambient Sound', *Journal of Atmospheric and Oceanic Technology*, vol. 7, no. 4, 1990, pp. 576–595, DOI:10.1175/1520-0426(1990)007<0576:AEOTWT>2.0.CO;2.

[30] Pensieri, S. et al., 'Underwater Acoustic Measurements to Estimate Wind and Rainfall in the Mediterranean Sea', *Advances in Meteorology*, no. 612,512, 2015, DOI:10.1155/2015/612512, (PAGE REF?)

[31] Commission Decision, 'Laying Down Criteria and Methodological Standards on Good Environmental Status of Marine Waters and Specifications and Standardized Methods for Monitoring and Assessment, and Repealing Decision 2010/477/EU', *Official Journal of the European Union*, L125, 2017/848/EU, pp. 43–74.

[32] Hermannsen, L' et al., 'High Frequency Components of Ship Noise in Shallow Water with a Discussion of Implications for Harbor Porpoises (Phocoena Phocoena), *Journal of the Acoustical Society of America*, vol. 136, no. 4, 2013, pp. 1,640–1,653, DOI:10.1121/1.4893908.

Original Scientific Article • DOI: 10.2478/rmzmag-2021-0005

Received: October 01, 2021
Accepted: October 19, 2021

An analysis of coal consumption, CO_2 emissions and economic growth in Slovenia

Analiza porabe premoga, izpustov CO_2 in gospodarske rasti v Sloveniji

Aleš Budna, Goran Vižintin*

University of Ljubljana, Faculty of Natural Sciences and Engineering, Department of Geotechnology, Mining and Environment, Aškerčeva 12, Ljubljana, Slovenia

*Corresponding author: E-mail: goran.vizintin@guest.arnes.si

Abstract in English

The common characteristics and possible correlations between coal consumption, CO_2 emissions, emission productivity and economic growth in Slovenia are discussed in this article. The correlation between these variables was analysed by using the Pearson correlation coefficient, and we used linear regression and the least squares method to develop predictive mathematical models that can be used to estimate trends in coal consumption and CO_2 emissions in the future. The link between coal consumption, emissions, and emission productivity is significant, while the correlation between coal consumption and economic growth is minimal. Therefore, coal consumption and the resulting emissions do not have a significant impact on economic growth. Mathematical models show a good fit, which is a condition for the reliability of the prediction. Possible scenarios of the transition to carbon neutrality and the related problems of future electricity supply as a consequence of the cessation of coal mining and use are also discussed below.

Keywords: coal, emissions, correlation, forecasting

Abstract in Slovene

Obravnavane so skupne značilnosti in možne korelacije med porabo premoga, emisijami CO_2, emisijsko produktivnostjo in gospodarsko rastjo v Sloveniji. S Pearsonovim koeficientom korelacije se je analizirala povezanost med navedenimi spremenljivkami ter se s pomočjo linearne regresije in metode najmanjših kvadratov izdelalo napovedne matematične modele, s katerimi se lahko ocenijo trendi porabe premoga in emisij CO_2 v prihodnosti. Povezanost med porabo premoga, emisijami in emisijsko produktivnostjo je znatna, medtem ko je korelacija med porabo premoga in gospodarsko rastjo minimalna, zato poraba premoga in s tem emisije nimajo pomembnega vpliva na gospodarsko rast. Matematični modeli kažejo dobro prileganje, kar je pogoj za zanesljivost napovedi. V nadaljevanju so obdelani tudi možni scenariji prehoda na ogljično nevtralnost in s tem povezano problematiko prihodnje oskrbe z električno energijo kot posledico prenehanja pridobivanja in uporabe premoga.

Ključne besede: premog, emisije, povezanost, napovedovanje

Introduction

The main challenge facing many countries is the development of energy and environmental policies for the production of sustainable energy, while reducing greenhouse gas (GHG) emissions. As global energy demand continues to increase, energy security issues have become even more important.

Researching emission trends and predicting their further values is therefore an important part of adapting energy strategies, especially those involving low carbon. Understanding the dynamic link between coal consumption, CO_2 emissions and economic growth is therefore crucial in shaping energy strategies.

We would like to present the common characteristics and possible correlations between

coal consumption, CO_2 emissions, and economic growth in Slovenia, as well as develop predictive mathematical models that will assess the trend of coal consumption and CO_2 emissions in the future.

Materials and methods

Coal

Among fossil fuels, coal is the only source that will have the longest presence in the energy market due to the enormous number of reserves worldwide. As an energy source, it represents a quarter of the world share. In Europe, its consumption is declining while in the fast-growing Asian markets its consumption is quickly rising (Figure 1) [1]. However, the combustion of fossil fuels releases a lot of CO_2 into the atmosphere, which contributes to the greenhouse effect.

It is necessary to handle coal reserves and their exploitation in Slovenia as rationally as possible, because of all the fossil energy sources, Slovenia disposes only of coal. Energy obtained from coal represents a quarter of all electricity consumed in Slovenia. On the one hand, this represents a great burden on the environment, and on the other hand, it is a strong economic and social factor for both the region and the country [2].

After the cessation of excavation in the Trbovlje-Hrastnik Mine and the closure of the Trbovlje Power Station, Termoelektrarna Trbovlje (TET), the only two major consumers of coal for the production of electricity or heat (which is collectively called transmission) that remained in Slovenia are Termoelektrarna Šoštanj (TEŠ), which uses lignite from Premogovnik Velenje (PV), and the Ljubljana Power Station, Termoelektrarna-toplarna Ljubljana (TE-TOL)) which already replaces imported coal with wood chips and gas [3].

Coal consumption in Slovenia has been in decline for some time (Figure 2), and harmful emissions from the transmission sector have also decreased by about a quarter owing to more modern procedures and improvements [2].

CO_2 emissions

CO_2 is one of the most dangerous pollutants, which has a great impact on the environment and consequently on humans and all living things on Earth. The combustion of fossil fuels is the largest source of atmospheric CO_2.

Nowadays, production and consumption of CO_2 are out of balance; therefore, the CO_2 content in the atmosphere is increasing. The consequences of an increased concentration of CO_2 in the atmosphere are also called the 'greenhouse effect'.

The share of CO_2 emissions from coal combustion in Slovenia in the period observed is around 30% and is declining, mainly owing to reduced coal consumption but also to the replacement of fossil fuels, changes in the amount of carbon in coal, improved efficiency, and changes in the share of renewable sources and nuclear energy [5].

The National Energy and Climate Plan of Slovenia anticipates the phasing out of the use of domestic and imported coal for energy

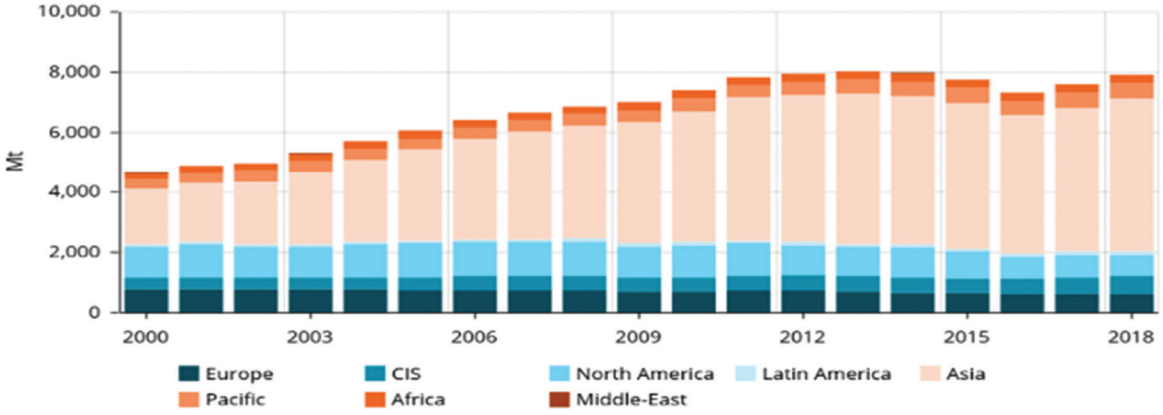

Figure 1: *Worldwide coal consumption [1].*

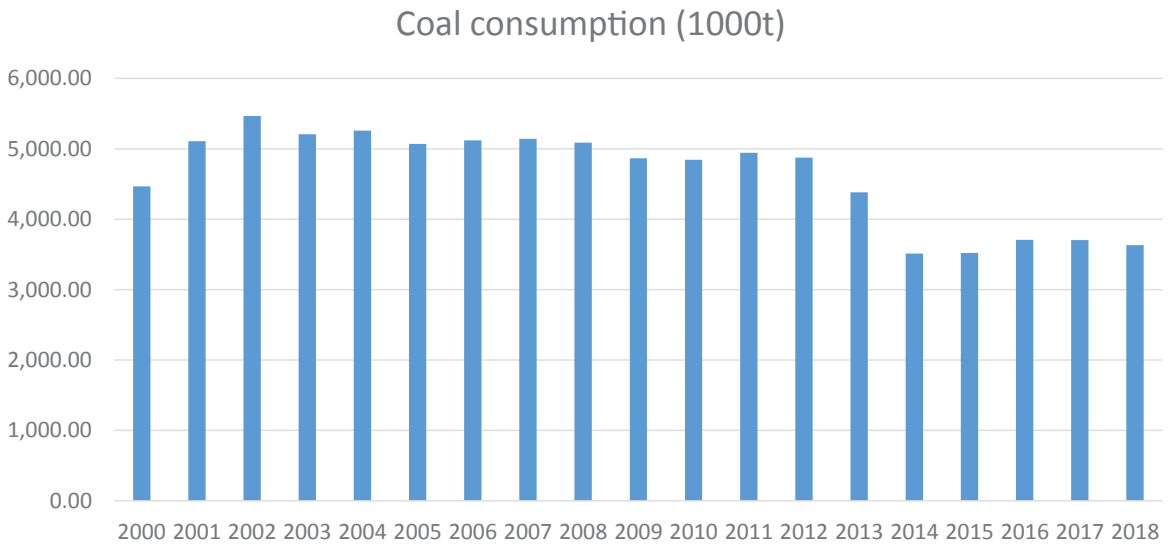

Figure 2: *Coal consumption in Slovenia [7].*

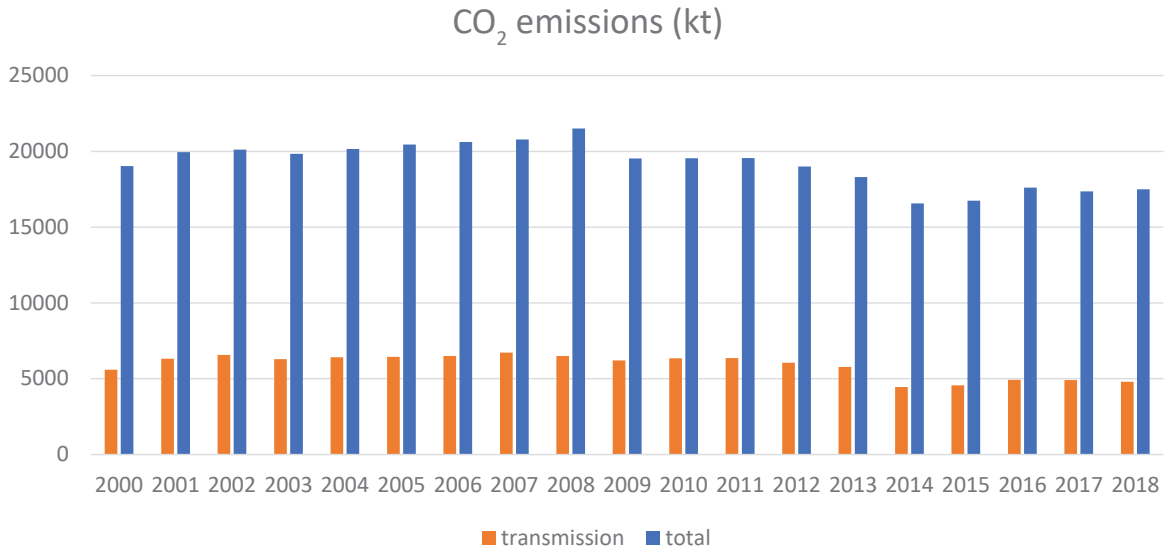

Figure 3: *Amount of CO_2 emissions [3].*

purposes or a reduction of at least 30% by 2030, as well as the reduction of total GHG emissions by up to 36% compared with 2005 [6].

Although the energy sector has great potential to reduce emissions, it must be acknowledged that it has already made a significant contribution to reducing them. In Slovenia, for example, emissions from the energy sector decreased by about 24 percent between 2005 and 2017, while such a decline has not been seen in any other sector; for example, transport emissions increased by 25 percent [2].

The largest sources of energy emissions (in 2015) are transportation (40%) and electricity and heat production (37%), while manufacturing contributes to 12% of the energy emissions, and households and the service sector together contribute to 11% of the energy emissions (Figure 3) [3].

The largest share in greenhouse gas emissions is CO_2 (96 %).

CO_2 is the equivalent of all greenhouse gases expressed in weight rates of CO_2.

Economic growth

Positive economic growth is one of the most important goals of any economy. Economic growth is measured by the growth rate of the gross domestic product (GDP) [8].

The share of transmission of the electricity produced is about one third, and the share of GDP is between 0.56 and 0.86 percent.

A comparison of the movement of GHG emissions from energy sources with the movement of the gross domestic product and energy supply shows whether the breakdown of GDP growth and emissions was achieved and what influenced the breakdown. The analysis showed that the breakdown was achieved mainly in the period 2002–2007 because of structural changes and more efficient energy use and in 2012–2014 because of a reduction in the share of fossil fuels in energy supply and greater energy efficiency (Figure 4) [3].

Emission productivity

Emission productivity is calculated as the quotient of the gross domestic product at constant prices and total greenhouse gas emissions (Figure 5). The key objective of the emission productivity indicator is to monitor the environmental performance of the economy.

Emission productivity in Slovenia is steadily growing and approaching the EU average.

In the future, it will be important that the indicator improves and ensures a breakdown between GDP and GHG growth. The goal is to significantly reduce GHG emissions while at the same time growing economically [3].

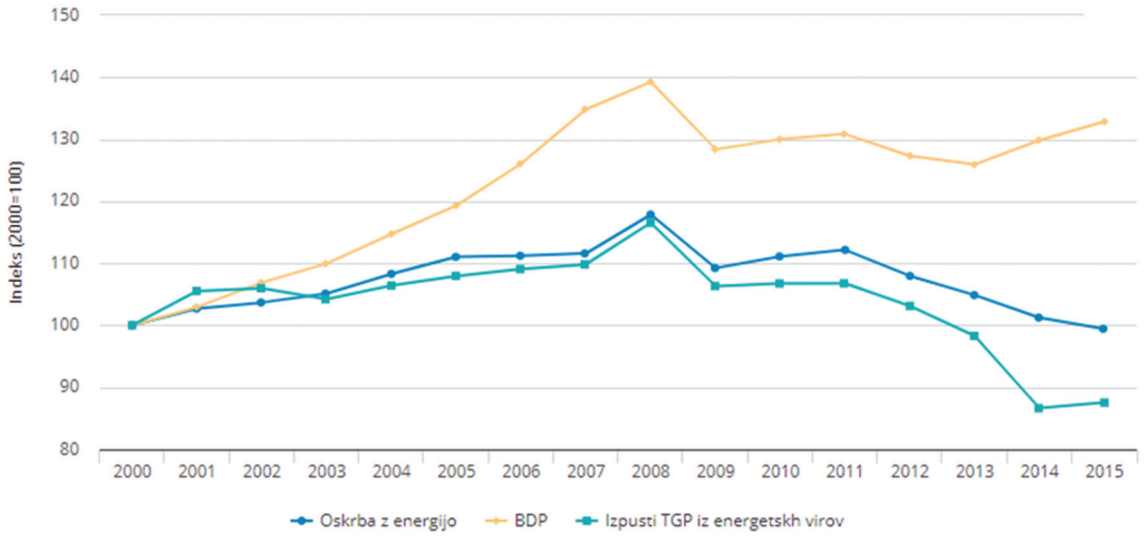

Figure 4: *Trends in GHG emissions from energy sources, gross domestic product and energy supply in the period 2000–2015 [3].*

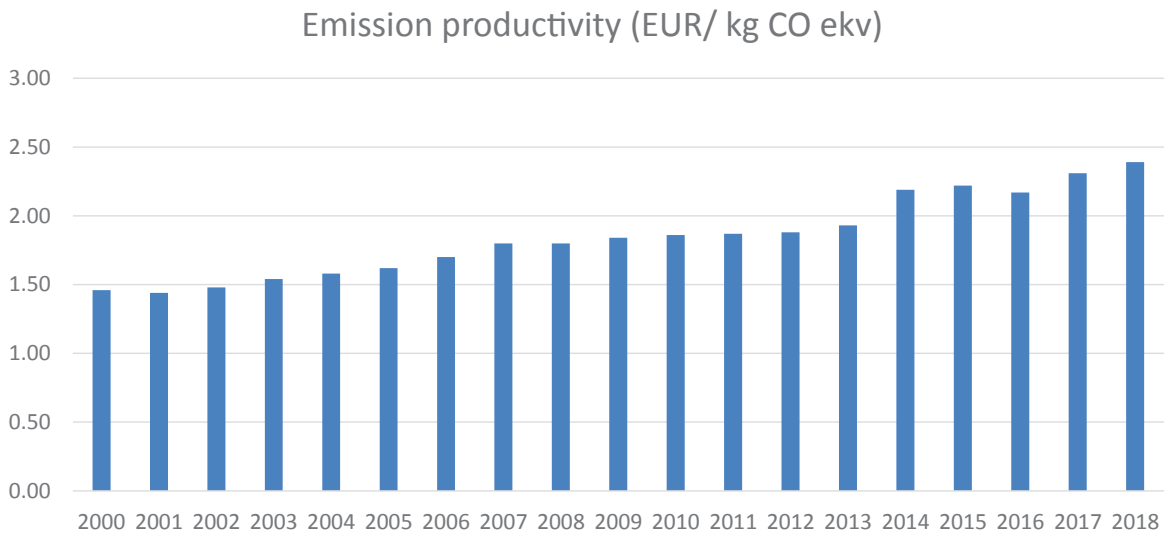

Figure 5: *Emission productivity in Slovenia [3].*

Pearson correlation coefficient

Correlation or the correlation coefficient is a numerical measure that represents the strength of the linear relationship of two variables.

The Pearson correlation coefficient is the most commonly used measure of the linear correlation of two numerical variables, calculated on the basis of the covariance and standard deviations of the set of both variables [9].

$$\rho = \frac{K(x;y)}{\sigma(x)\sigma(y)} = \frac{\sum_{i-1:N}(xi-\bar{x})(yi-\bar{y})}{\sqrt{\sum_{i-1:N}(xi-\bar{x})^2\left(\sum_{i-1:N}yi-\bar{y}\right)^2}} \quad (1)$$

K(x;y) represents the covariance, and the σ values represent the standard deviation for the variables *x* and *y* [9].

Pearson correlation values are called the correlation index or strength, which can assume a value between -1 and 1 (Figure 6).

An is some extreme value relative to other data and that does not match the general data trend. One method of determining outliers is the visual perception of the extreme value in the graph itself (Figure 7) [11].

Simple linear regression

The fit of an appropriate mathematical model to data is called regression, which can be simple or complex. We are looking for relations between the independent and dependent variable.

Simple linear regression is the simplest and most commonly used form of linear regression, where a regression line is used to study the effect of only one independent variable *X* on *Y*.

The goal of the regression is to calculate the values of the parameters so that the model will best describe the data or fit them optimally. This means that the vertical deviations of the actual points from the model must be as small as possible (Figure 8) [10].

$$e_i = \hat{y}_i - y_i = min \quad (2)$$

Because some deviations are positive and some are negative, we square them. The criterion for minimising the sum of the squared deviations is called the Ordinary Least Squares method (OLS) [12].

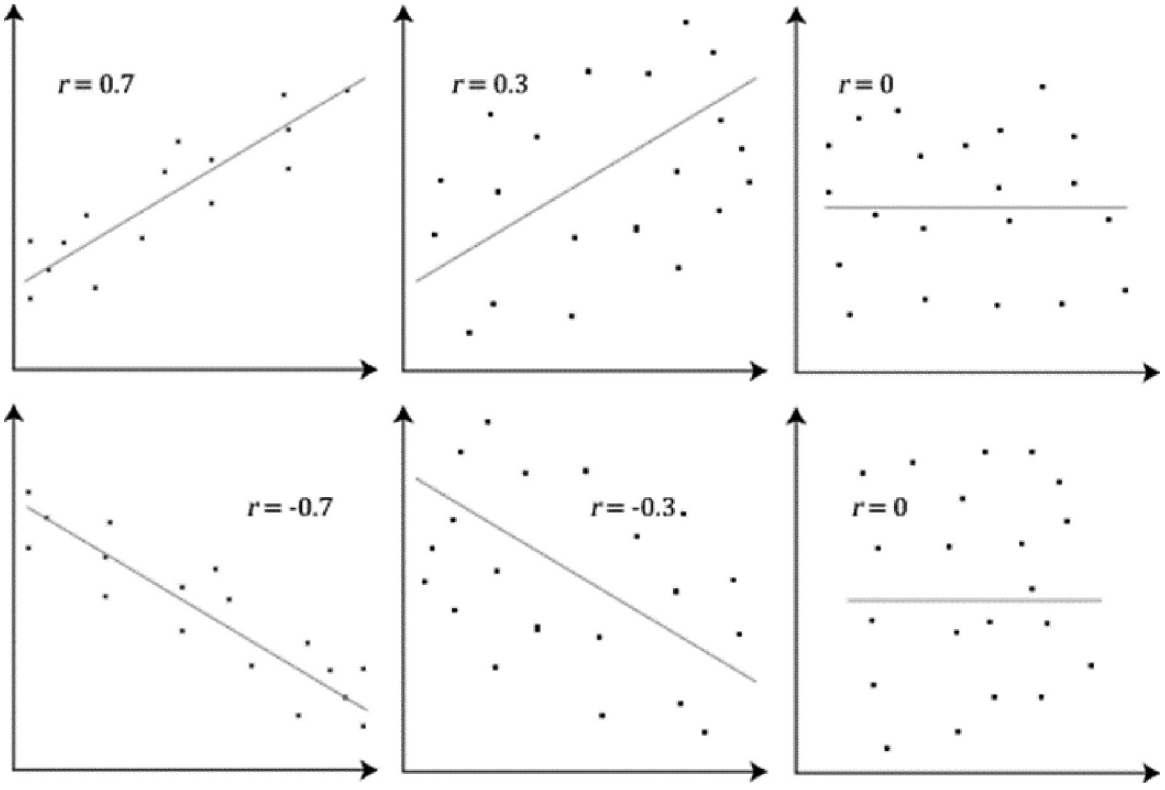

Figure 6: *Correlation coefficient strength [10].*

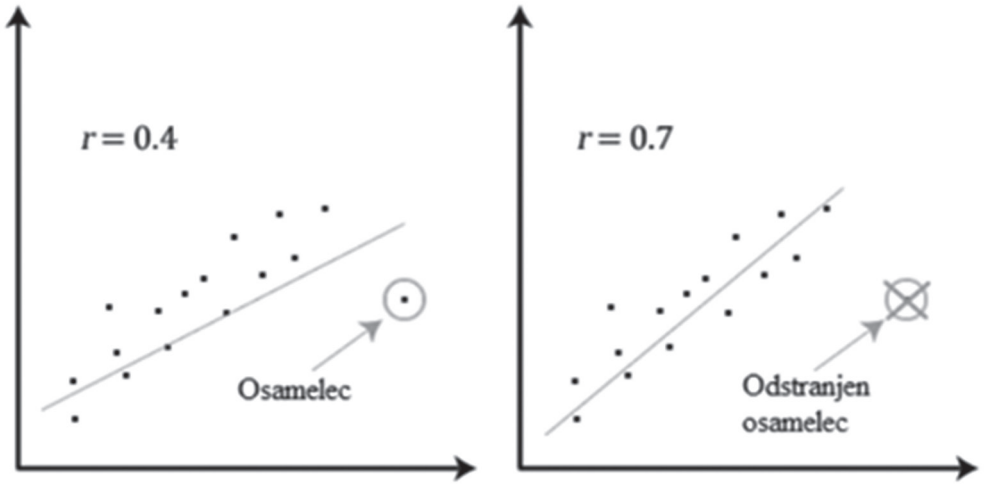

Figure 7: *Removing the outlier [11].*

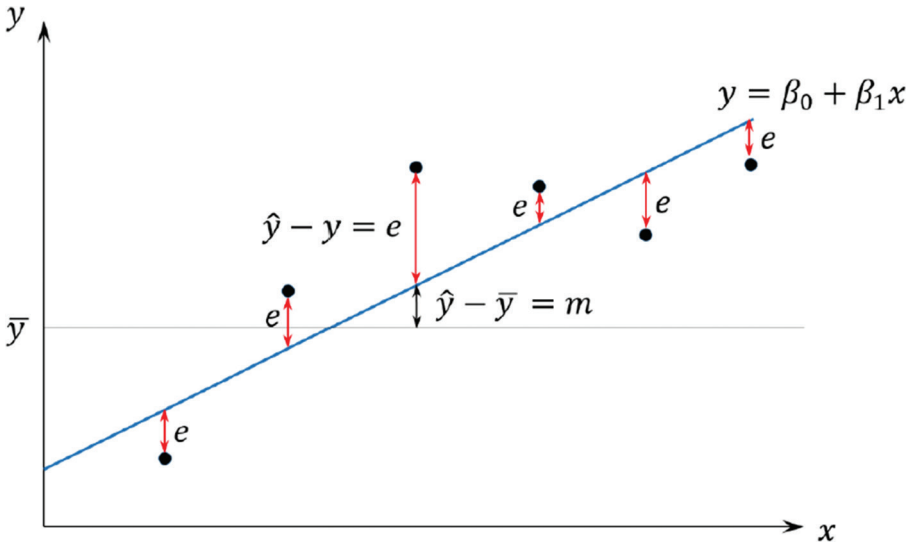

Figure 8: *Deviations of points from the line and deviation of the line from the mean [10].*

In the case of an *n*th degree polynomial, we look for *n* + 1 parameters, with which we try to best approximate the measurements (Figure 9).

$$\hat{d}(t) = \hat{a}t + \hat{b} \rightarrow \begin{cases} \hat{d}(1) = \hat{a} * 1 + \hat{b} \\ \dots \\ \hat{d}(N) = \hat{a} * N + \hat{b} \end{cases} \rightarrow \begin{bmatrix} \hat{d}(1) \\ \dots \\ \hat{d}(N) \end{bmatrix}$$

$$= \begin{bmatrix} 1 & 1 \\ 2 & 1 \\ 3 & 1 \\ \dots & 1 \\ N & 1 \end{bmatrix} = \begin{bmatrix} \hat{a} \\ \hat{b} \end{bmatrix} \quad (3)$$

$$\hat{d}(t) = \hat{a}t^2 + \hat{b}t + \hat{c} \rightarrow\rightarrow$$

$$\begin{cases} \hat{d}(1) = \hat{a} * 1^2 + \hat{b} * 1 + \hat{c} \\ \dots \\ \hat{d}(N) = \hat{a} * N^2 + \hat{b} * N + \hat{c} \end{cases}$$

$$\rightarrow \begin{bmatrix} \hat{d}(1) \\ \dots \\ \hat{d}(N) \end{bmatrix} = \begin{bmatrix} 1^2 & 1 & 1 \\ 2^2 & 2 & 1 \\ 3^2 & 3 & 1 \\ \dots & \dots & 1 \\ N^2 & N & 1 \end{bmatrix} = \begin{bmatrix} \hat{a} \\ \hat{b} \\ \hat{c} \end{bmatrix} \quad (4)$$

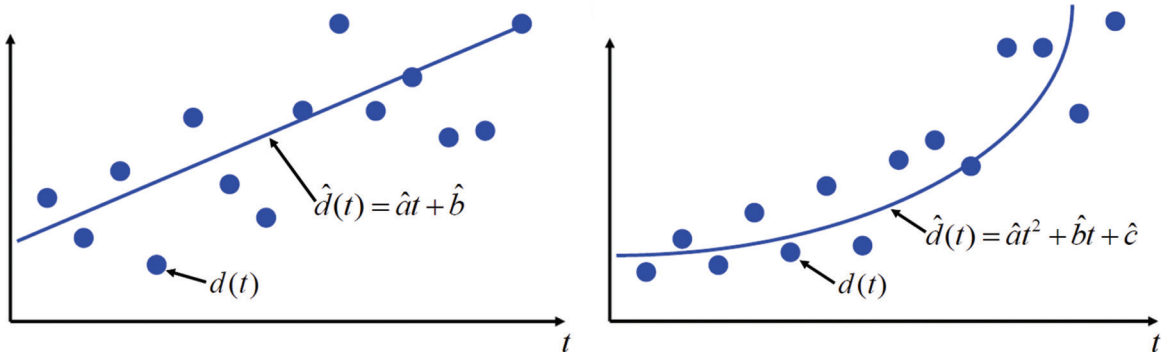

Figure 9: *1st- and 2nd-order linear regressions [10].*

The regression model can be better or worse, and the quality of the model can be evaluated in different ways. One of the simplest measures to evaluate the quality of a regression model is the coefficient of determination [12].

$$\Sigma(y_i - \bar{y})^2 = \Sigma(\hat{y}_i - \bar{y})^2 + \Sigma(\hat{y}_i - y_i)^2 \quad (5)$$

or

$$SST = SSR + SSE \quad (6)$$

The coefficient of determination R^2 is the ratio between SSR and SST.

$$R^2 = \frac{SSR}{SST} = 1 - \frac{SSE}{SST} \quad (7)$$

SST: sum of squared deviations,
SSR: total correction of the sum of squares and
SSE: model sum error.

The values of the coefficient of determination range from $0 \leq R^2 \leq 1$. The closer to the value of 1, the smaller the deviation between the actual points and the model [10].

Another indicator of the reasonableness of fit is the presentation of residues compared with the independent variable. Residues must be randomly distributed and contained in a relatively small band, which is proportional to the accuracy of the data [4].

The relationship between coal consumption and transmission of CO_2

The correlation between coal consumption and CO_2 emissions generated directly by transmission is a very high positive relationship: *r = 0.98*.

The correlation between CO_2 emissions and economic growth and between coal consumption and economic growth is small and negative (-0,23274 or –0,36466), which means that the impact of coal consumption – and thus also transformational emissions – on economic growth is minimal, that is, coal consumption does not have a large impact on economic growth, which is typical for developed countries, where the 'black industry' is no longer a driver of development. The minus sign, however, means inverse connectivity, ie that by reducing coal consumption and CO_2 emissions, gross domestic product grows.

We calculate the linear regression equation (Figure 10), which in this case is a 1st-order equation, or a linear line in which *y* represents CO_2 emissions and *x* represents coal consumption.

$$y = 1{,}110555x + 745{,}027 \quad (8)$$

In this case, the fitting of the mathematical model is $R^2 = 0.96$. Since the value of the coefficient of determination is very close to 1, the suitability of the model is very high. The residue graph does not show a visible trend.

The relationship between coal consumption and total CO_2 emissions

The correlation between coal consumption and total CO_2 emissions, which are defined as the sum of emissions from transport, energy, industrial processes, fuels in manufacturing, agriculture, waste, other sectors, fugitive emissions from fuels, and others, also indicates a high positive relationship *r* = 0.93 between coal consumption and total CO_2 emissions, as the transmission sector accounts for almost a third of the total emissions.

The calculation gives the linear regression equation (Figure 11), which in this case is an equation of the 1st order, or a linear line with the equation:

$$y = 2{,}002699x + 9908{,}849 \quad (9)$$

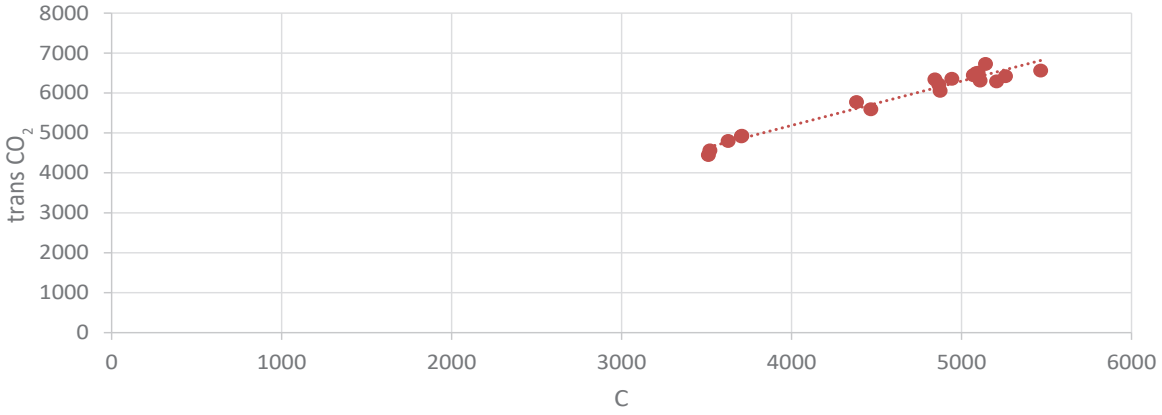

Figure 10: *Emissions of transmission depending on the use of coal.*

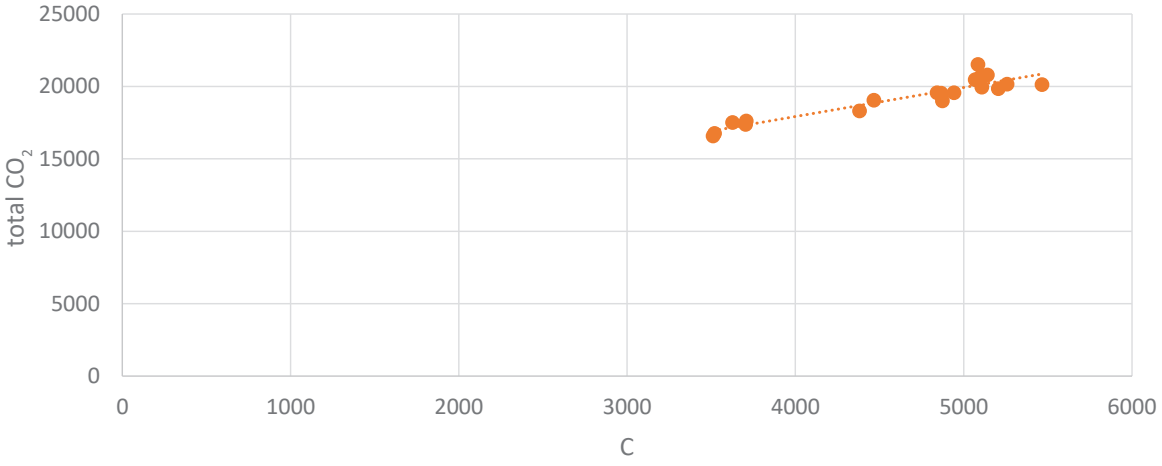

Figure 11: *Total emissions depending on coal consumption.*

where y represents the total emissions and x represents coal consumption.

The fit of the mathematical model is defined by the coefficient of determination R^2, which in our case is $R^2 = 0.87$. The value of the coefficient of determination is quite close to 1, which means that the suitability of the model is high to very high.

Another indicator of the reasonableness of fit is the display of residues compared with the independent variable. The residual graph shows a random distribution without a visible trend, which is also a condition for the suitability of the model.

The relationship between coal consumption and emission productivity

Emission productivity is calculated as the ratio between the gross domestic product at constant prices and all greenhouse gas emissions expressed in eq. CO_2.

In the analysis of the graph, a point that stands out from the trend of the model, which we call the outlier (year 2000), is noticed. We eliminate this point and start with 2001 and continue with the calculations (Figure 12).

The correlation coefficient increased from –0.86145 to -0.92875, that is, the connectedness of the data is now just under 7% better.

The calculation of the Pearson correlation coefficient shows a very high negative correlation, $r = -0.93$, between coal consumption and emission productivity. The strength of the connection is high and inversely proportional, which means that coal consumption has a strong impact on emission productivity in the sense that the lower the coal consumption, the higher the emission productivity.

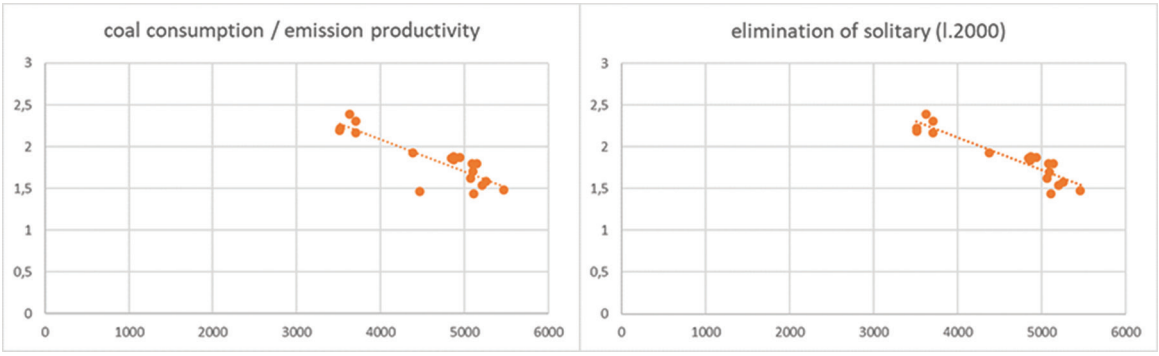

Figure 12: *Elimination of the outlier.*

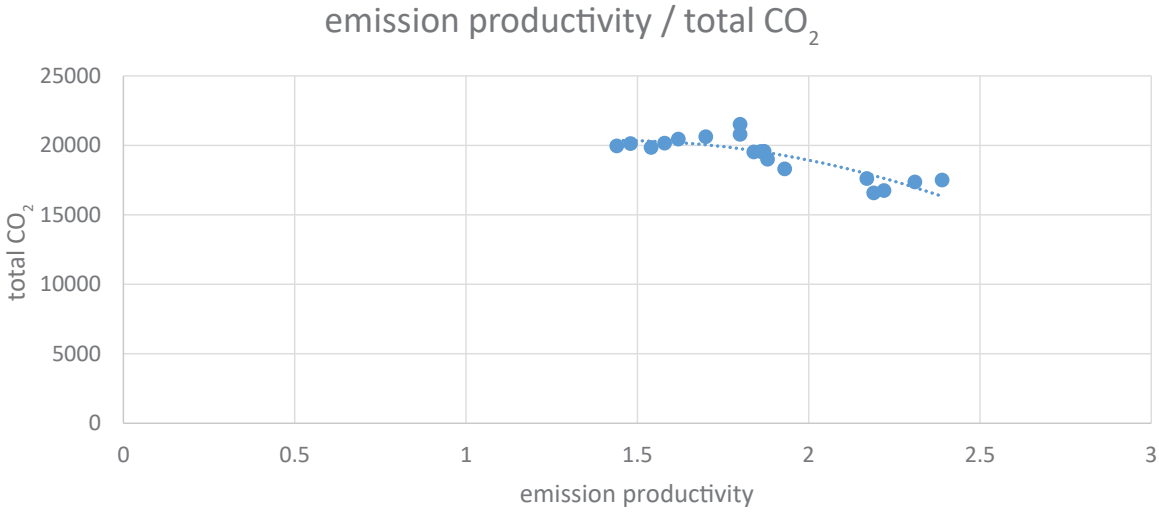

Figure 13: *Emission productivity in relation to total emissions.*

The calculation gives the linear regression equation, where y is the emission productivity and x is the coal consumption, which in this case is a first-order equation or linear line with the following equation:

$$y = -0.00039x + 3.671887 \qquad (10)$$

The fit of the mathematical model is defined by the coefficient of determination R^2, which in our case is $R^2 = 0.86$. The display of residues compared with the independent variable also shows the degree of relevance of the model.

The relationship between productivity and the emission of total CO_2 emissions

The correlation between emission productivity and total CO_2 emissions shows a high negative correlation, which leads us to the fact that with increasing emission productivity, total CO_2 emissions fall. The Pearson correlation coefficient is $r = -0.82$.

A connectedness in the form of an inverse U curve is noticeable, so we set the mathematical model as a linear regression of the second order, or a quadratic regression.

The calculation gives a mathematical model in functional form:

$$y = -4,402.5x2 + 12615.56x + 11,320.67 \qquad (11)$$

In this model, y represents total emissions and x represents emission productivity.

The fit of the mathematical model is defined by the coefficient of determination R^2, which in our case is $R^2 = 0.73$. The residual graph does not show a visible trend, which is also a condition for the suitability of the model.

Withdrawal from coal

The strategy of withdrawing from coal or the closure of the Velenje Mine and thus the cessation of TEŠ's operation, as well as the work

of various restructuring groups and presentations of various studies, both on the governmental and non-governmental side, imply that 2033 or 2050 would be possible years to completely end coal consumption, where 2033 is a governmental prediction and 2050 is a prediction made by employee representatives and the energy professionals. The following two reasons were crucial for such a decision: changing external circumstances, especially the increase in emission coupon prices (and price projections until 2030), together with the increase in climate targets at the EU level, which significantly increase the risk of uneconomical operation of TEŠ; and that such a scenario has the most positive effects on climate, local environment, nature, and human health. Such a decision is also influenced by the possibility of drawing funds from the European Fund for a Fair Transition.

However, such a rapid and uncontrolled withdrawal from coal would also be problematic from the point of view of a reliable supply of electricity produced in Slovenia, as it would be difficult to plan replacement capacities in time, as well as from the point of view of employees and the closure process of Premogovnik Velenje.

The share of electricity that would be lost in this way cannot be replaced with renewable sources in a short time, especially because TEŠ is also the most important domestic source, which can adapt to most unpredictable situations in the electricity system and provide a range of system services. At the same time, it also produces thermal energy for the needs of consumers in the Šalek Valley and thus supplies the second largest hot water system in the country. It should also not be forgotten that in the event of the imminent shutdown of TEŠ, import dependence would also increase sharply, averaging around 17 percent of electricity in recent years, in view of forecasts of growing demand for electricity in the future.

Among several possible energy sources that would be an energy alternative to fossil fuels and would continue to use the energy location at TEŠ, one is gas, whilst others may be some alternative sources for which it would be difficult to compensate for the lack of electricity in a short time. Gas and alternative fuels, where we have Solid Recovered Fuel, have a half lower emission factor (the ratio between CO_2 emissions and net calorific value expressed in kg CO_2/GJ), which means that when we burn these, half as many CO_2 emissions are produced as with coal combustion. The use of gas is not economically justifiable for now, and the local community opposes the incineration of Solid Recovered Fuel. Even the reserves in hydropower, which are supposed to mitigate the outage in the beginning, would not be sufficient in the long run.

The solution proposed by employees for closing the mine as late as possible is also to redirect the funds paid by TEŠ through CO_2 coupons to the Climate Change Fund, whose funds are intended for climate change mitigation, to solve the problem of closing the Velenje Coal Mine and the region. The funds raised in this way would be used to improve and reduce the environmental footprint by capturing carbon, new technologies, environmental policies and for the needs of regional development policies.

We will have to take care of our self-sufficiency, and we will need another major conventional source in the long run, so the decision on long-term use of nuclear energy is also important, which some decision makers believe is the only real solution to replace energy production from thermal power plants. There are several obstacles with this as well, including the fact that the construction of a nuclear power plant is expensive and time-consuming, so it may be that we would have to wait a very long time for electricity from this source.

In shaping Slovenia's energy future, we will need an appropriate mix of energy sources that will provide us with a safe and reliable supply of low-carbon energy at affordable prices.

In addition to the benefits, the withdrawal from coal consumption also brings problems that need to be solved. Not only is it necessary to compensate for the loss of electricity production with other sources, but it is also necessary to take care of areas that have so far lived off the coal industry. The problem is not only the renewed employment of the people who have worked in this industry, but the economic restructuring of the entire economy of these areas. Finally, we must also invest in the rehabilitation of the environment left behind by the coal industry.

Conclusion

Coal consumption in Slovenia has been on a declining trend for quite some time, harmful emissions from the transmission sector have also decreased by about a quarter due to more modern procedures and improvements. On the other hand, total GHG emissions are not decreasing; rather, they are increasing slightly, mainly owing to a large increase in transport emissions. Emission productivity is growing steadily and is approaching the EU average. If in the last century coal was still a driver of development in Slovenia and its impact on economic growth was significant, nowadays there is a noticeable gap between GDP and coal consumption, which is a characteristic of developed countries.

Using mathematical modelling and setting up mathematical models to predict the behaviour of certain dependent parameters in the future, we can predict how the parameters observed will react to changes. In general, models can only approximate behaviour in the real world.

The National Energy and Climate Plan of Slovenia anticipates the phasing out of the use of domestic and imported coal for energy purposes, which means that we will have to develop an appropriate energy strategy in the future that will ensure a safe and reliable supply of low-carbon energy.

References

[1] Enerdata – Yearbook [online]. Available on: https://yearbook.enerdata.net/coal-lignite/coal-world-consumption-data.html.

[2] Dervarič, E., Medved, M., Klenovšek, B. 'Globalna Ocena Svetovnih Trendov Pri Proizvodnji In Prodaji Energetskega Premoga – Projekcije Proizvodnje Energetskega Premoga V Republiki Sloveniji', *Posvetovanje rudarskih in geotehnoloških strokovnjakov ob 41. Skoku čez kožo*, 2006, p. 33.

[3] ARSO, 'Agencija RS za okolje' http://kazalci.arso.gov.si/. (AUTHOR, COMPLETE REFERENCE)

[4] Giordano, F.R., Fox, W.P., Horton, S.B., *A First Course in Mathematical Modeling*, (5th ed.) Boston, MA, Cengage Learning,, 2013, (PAGE REF?)

[5] Kortnik, J., *Okoljski Inženiring Skripta*, Faculty of Natural Sciences and Engineering, Department of Geotechnolgy, Mining and Environment, Ljubljana, University of Ljubljana,: 2016, p. 114.

[6] Vlada Republike Slovenije, *Celoviti Nacionalni Energetski in Podnebni Načrt Republike Slovenije*, http://www.vlada.si/(AUTHOR, COMPLETE REFERENCE)

[7] SURS – Statističen Urad RS, https://www.stat.si/StatWeb/, (AUTHOR, COMPLETE REFERENCE)

[8] Ekonomski Sistemi in Ekonomska Politika, Kombre, K. https://vs-kombre.kk.edus.si. (AUTHOR, COMPLETE REFERENCE)

[9] Zemljak, D. *Korelacijska Analiza*, MA diss., University of Maribor, Maribor, Faculty of Natural Sciences and Mathematics, Department of Mathematics and Computer science 2019, (PAGE REF?)

[10] Novina, U. (2016): *Načrtovanje Prototipa Sistema Za Napovedovanje v Excelu In Njegova Uporaba v Logistiki.* MA Diss. Maribor, University of Maribor, Faculty of Logistics, (PAGE REF?)

[11] Novina, U., *Pearsonov Koeficient Korelacije*, https://urosnovina.weebly.com/blog/pearsonov-koeficient-korelacije, 2017 (AUTHOR, COMPLETE REFERENCE)

[12] Pal, A., *Prispevek k Razvijanju Modificirane Sigmoidne Funkcije, Uporabljene Za Modeliranje Posedanja, Ki Je Posledica Vpliva Podzemnega Rudarjenja*. Master's Thesis. Ljubljana, University of Ljubljana, Faculty of Natural Sciences and Engineering, Department of Geotechnology, Mining and Environment, 2017 (PAGE REF?)

Original Scientific Article • DOI: 10.2478/rmzmag-2021-0006

Received: October 21, 2021
Accepted: November 26, 2021

Determination of material quality by methods of thermal analysis

Ugotavljanje kakovosti materiala z metodami termične analize

Maja Vončina[1,*], Gregor Hvala[1], Jožef Medved[1], Borut Žužek[2], Mitja Petrič[1]

[1]University of Ljubljana, Faculty of Natural Sciences and Engineering, Department of Materials and Metallurgy, Ljubljana, Slovenia

[2]Institute of Metals and Technology, Lepi pot 11, 1000 Ljubljana, Slovenia

*Corresponding author: E-mail: maja.voncina@ntf.uni-lj.si

Abstract in English

Cast aluminium alloys are commonly used in the automotive industry for casting applications. There are both primary and secondary/recycled aluminium alloys in the market, which differ in price and quality. In this study, the effect of alloy quality on solidification, microstructure and mechanical properties was investigated. The comparison of properties was carried out in the as-cast condition and in the heat-treated condition. The influence of alloy quality on solidification was analysed by simple thermal analysis and differential scanning calorimetry, and thermodynamic simulations. The basic mechanical properties analysed were tensile strength, yield strength, elongation, and hardness. The microstructural differences were analysed using a light microscope. The Mn:Fe ratio, which is strongly influenced by the alloy quality, was found to have a pronounced effect on the mechanical properties, while magnesium together with silicon hardens the aluminium matrix during heat treatment, which significantly increases the mechanical properties.

This research proved that thermal analysis methods can give us a necessary and important indication of the quality of the alloys used.

Keywords: Alloy quality, casting alloys, thermal analysis, solidification, microstructure, mechanical properties

Abstract in Povzetek

Aluminijeve zlitine se pogosto uporabljajo v avtomobilski industriji pri vlivanju. Na trgu obstajajo primarne in sekundarne/reciklirane aluminijeve zlitine, ki se razlikujejo po ceni in kakovosti. V tej študiji je bil raziskan vpliv kakovosti zlitine na strjevanje, mikrostrukturo in mehanske lastnosti. Primerjava lastnosti je bila narejena v litem in v toplotno obdelanem stanju. Vpliv kakovosti zlitine na strjevanje smo analizirali z enostavno termično analizo in diferenčno vrstično kalorimetrijo ter termodinamičnimi simulacijami. Analizirane so bile osnovne mehanske lastnosti, kot so natezna trdnost, meja tečenja, raztezek in trdota. Mikrostrukturne razlike smo analizirali z optičnim mikroskopom. Dokazano je, da razmerje Mn:Fe, na katerega močno vpliva kakovost zlitine, izrazito vpliva na mehanske lastnosti, medtem ko magnezij skupaj s silicijem med toplotno obdelavo utrjuje aluminijasto matrico, kar tudi bistveno poveča mehanske lastnosti.

V tej raziskavi je bilo dokazano, da nam lahko metode termične analize dajo potreben in pomemben podatek o kakovosti uporabljenih zlitin.

Ključne besede: kakovost zlitin, livarske zlitine, termična analiza, strjevanje, mikrostruktura, mehanske lastnosti

Introduction

One of the few disadvantages of aluminium is its expensive and energy-intensive extraction. It is mainly extracted from bauxite ore by the Bayer process. This produces alumina (Al_2O_3), from which technically pure aluminium is later extracted by electrolysis. An alternative to this extraction method is secondary extraction, that is, recycling, which requires only about 10% of the energy needed to produce one tonne of primary aluminium. The disadvantage of recycling

is the slightly higher content of some elements, the removal of which is extremely difficult or inadvisable. One such element is iron, which is otherwise required in the die casting of aluminium alloys because it prevents the castings from soldering to the tool. However, too much iron can deteriorate the alloy's mechanical properties.

The addition of magnesium to Al-Si alloys is the basis for the group of alloys characterized by exceptional castability and excellent mechanical properties after heat treatment. They are corrosion resistant and thermal expansion is low. Magnesium is added to binary alloys to improve the properties after heat treatment T6, which is characteristic of this type of alloy, through the mechanism of precipitation hardening. The heat treatment consists of solution annealing, quenching, and artificial aging, during which the hardening intermetallic phase Mg_2Si precipitates. The mechanical properties can be further improved by the addition of manganese and beryllium, which affect the morphology of the iron-based phases, improving the strength properties and ductility [1, 2]. The best effect of magnesium addition is seen at a content between 0.2 and 0.6% by weight, very rarely exceeding 1% by weight. The lower limit is determined by a sufficient amount for precipitation of the Mg_2Si phase, so that the effect on the mechanical properties is noticeable. The upper limit is determined by a still satisfactory plasticity; there should not be too much Mg_2Si phase in the microstructure. The magnesium content has a great influence on aging, so that the permissible limits in the individual alloys are very narrow. They also depend very much on the other alloying elements and the expected aging regime of the alloy [3, 4].

Solidification of AlSi10Mg and AlSi10Mg(Fe) alloys depends largely on the cooling rate and alloying elements, and usually begins in the temperature range between 550 °C and 600 °C. Solidification of this type proceeds as follows: First, the primary aluminium α-Al crystals solidify at T_L. Further eutectic (α-Al + β-Si) is formed, meanwhile, the remaining melt is enriched with the other elements, leading to the formation of different intermetallic phases. The first to solidify are the Fe-phases α-$Al_{15}(Fe,Mn)_3Si_2$ and β-Al_5FeSi, and among the latter, the Mg-phase Mg_2Si solidifies. The proportion and ratio of these phases depend on the ratio of manganese and iron in the alloy [5, 6, 7].

Strength properties increase significantly after heat treatment compared to as-cast condition. The elongation at yield strength decreases. Compared to alloys with different iron contents, the solidification rate has a great influence. The hardness is higher in the secondary alloy due to the higher iron content [3, 4, 8, 9].

Inferior alloys may contain up to twice as much iron. Two Fe-phases form in cast aluminium alloys, namely, α-$Al_{15}(Fe,Mn)_3Si_2$ and β-Al_5FeSi. The former is more desirable due to its rounded shape in the microstructure, as it does not adversely affect the mechanical properties like β-Al_5FeSi. Therefore, manganese is added to the alloys to convert the needles of the β-Fe_5FeSi phase to the α-$Al_{15}(Fe,Mn)_3Si_2$ phase. The optimum Mn:Fe ratio in the alloys was found to be about 0.5 [10].

Materials and methods

Based on the chemical composition of the studied alloys, listed in Table 1, a simulation of Scheil's thermodynamic non-equilibrium solidification was performed, using Thermo-Calc software and the TCAL6 database. Alloy AlSi10Mg is marked as 239, with better and purer quality, and alloy AlSi10Mg(Fe) as 239D, of inferior quality.

To characterize the solidification path of two alloys under investigation, the samples were melted in an induction furnace in a steel crucible coated with BN-foundry coating. The experimental alloy was preheated to 700 °C. After completion of the melting process, the experimental samples were then cast at a temperature of 700 °C in a Croning measuring cell, where the cooling rate was ~ 7 K/s and cooling curves were recorded. To characterize the accurate solidification of the test alloys, corresponding initial derivatives were obtained from the cooling curves. At the same time, the melt was also poured into a square steel mould (Figure 1), from which four specimens were obtained for the tensile tests.

Differential scanning calorimetry (DSC) analyses were also carried out to determine the

Table 1: *Chemical composition of the alloys investigated in % by weight.*

Sample	Si	Fe	Cu	Mn	Mg	Ni	
239	10.398	0.3548	0.005	0.2654	0.5513	0.0038	
239D	10.439	0.8788	0.0229	0.3092	0.4459	0.0062	
Sample	Zn	Pb	Sn	Ti	Sr	Al	Mn:Fe
239	0.0039	0.001	0.0003	0.0983	0.0369	rest	0.748
239D	0.0167	0.001	0.0004	0.0253	0.0015	rest	0.352

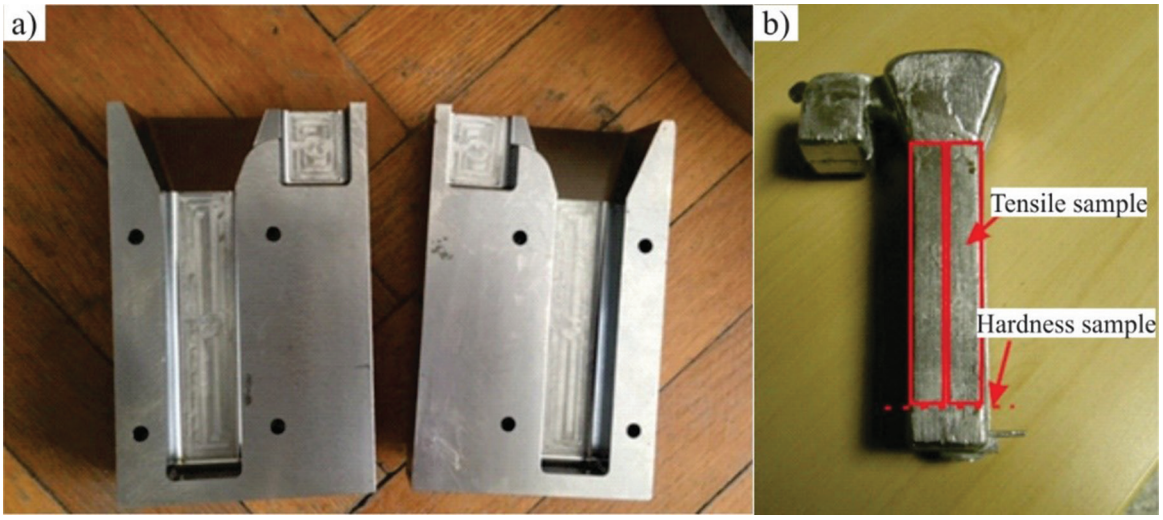

Figure 1: *(a) Steel mould with a square profile; (b) Casting obtained from the steel mould for tensile specimens.*

temperature changes and thermal effects occurring during heating / melting and cooling / solidification of the alloys studied. The experiments were carried out using a STA Jupiter 449C instrument from Netzsch by placing two identical corundum crucibles on the platinum sensor. The sample under investigation was placed in one crucible and an (inert) reference sample in the other. The system was heated to 720 °C in a furnace according to the preprogrammed temperature programme. It was kept at this temperature for 10 minutes. The heating and cooling phases were performed at a constant rate of 10 K / min. The test was performed in a protective atmosphere of Ar 6.0. During the measurement, the instrument recorded the temperature, the temperature difference between the tested sample and the reference sample, and the time. DSC analysis was performed on cast samples taken from the centre of the casting from Croning measurement cell [11]. The samples were turned to a diameter of 4.5 mm and a height of 4 mm and inserted into the instrument where the analysis was performed. After the measurements, the heating and cooling curves of the DSC were recorded, while the characteristic temperatures were determined from the heating and cooling curves of the DSC.

Specimens for microstructure investigations were prepared metallographically from the center of the casting from the Croning measuring cell [11] and photographed with a BX61 light microscope to analyze the effect of alloy quality on the formation and distribution of microstructural constituents.

Specimens of B 6 x 30 mm type were used for the tensile test, prepared according to DIN 50125: 2016-12. Four specimens of each test alloy were prepared in as-cast and T6 heat-treated condition. Tensile tests were carried out on INSTRON 8802 apparatus in accordance with SIST EN ISO 6892-1:2020 A224 standard.

To analyse the hardness of two grades of alloy in the as-cast and heat-treated condition,

the instrument NEXUS 7500 was used and the measurements were made in accordance with the standard SIST EN ISO 6506 - 1: 2014. A tungsten carbide ball with an HBW of 2.5 / 62.5 was used. Hardness measurements were carried out on specimens from a square-profile steel mould.

Results and discussion

Figure 1a shows the calculated cooling curve of sample 239 and Figure 2b shows the calculated cooling curve of sample 239D, where the dashed line indicates the equilibrium solidification. The results show that in sample 239 both Fe-phases solidify after the primary α-Al crystals and eutectic (α-Al + β-Si). It does not end with the Fe-phase β-Al_5FeSi; the phases π-$Al_8Si_6Mg_3Fe$ and Mg_2Si also solidify from the melt. The main difference between the investigated alloys is that at the alloy 239D the solidification of both Fe-phases occurs before the solidification of eutectic (α-Al + β-Si), whereas also the amount of those phases is much higher, respectively. The solidus temperature T_S is 554.7 °C for sample 239 and 555.1 °C for sample 239D.

The main difference between the samples / alloys in solidification, calculated with the Thermo-Calc program, is seen in the sonification path and proportions of each phase (Table 2). The calculated amount of Fe-phase α-$Al_{15}(Fe,Mn)_3Si_2$ in sample 239D is about twice that in sample 239, and an even greater difference occurs for the β-Al_5FeSi phase; it is up to 150% higher than in sample 239.

The cooling curves in Figure 3 show that the T_L in sample 239 is higher and the solidification interval is wider, which is consistent with Scheil's non-equilibrium solidification curve. This is followed by the solidification of the Fe-phases, the onset of which is indicated by T_1. This was determined from the derivative where the cooling rate is high, followed by a drop in the cooling rate due to the release of latent heat. This is followed by solidification of the eutectic with Fe-phases, namely α-$Al_{15}(Fe,Mn)_3Si_2$ and / or β-Al_5FeSi. Undercooling after the onset of eutectic solidification is illustrated by the temperature $T_{E/min}$, latent heat is released by the solidification and the temperature increases to $T_{E/max}$. The solidification proceeds in the same way until the temperature T_2, which was observed only for sample 239. Using calculations with Thermo-Calc, the eutectic solidification of the π-$Al_8Si_6Mg_3Fe$ phase can be predicted. The point T_3 represents the beginning of the solidification of the Mg_2Si eutectic phase. The final solidification temperatures (solidus temperatures) are much lower than those theoretically determined by the Scheil simulation of non-equilibrium solidification.

The results of the DSC analysis are shown in Figure 4 and show both the heating (green) and cooling (blue) curves for both samples tested. In both figures, the first inflexion point is at about

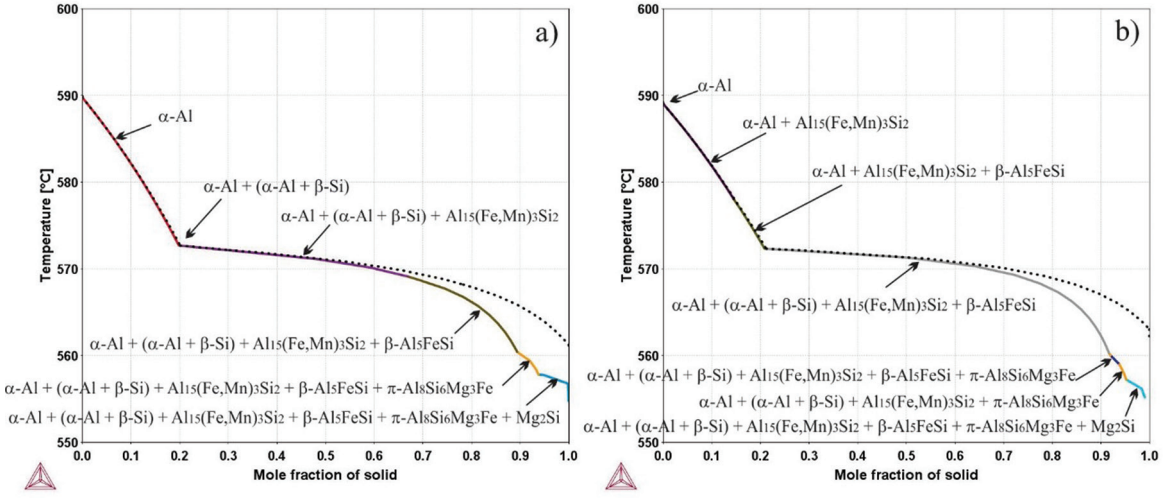

Figure 2: *The Scheil cooling curve of the non-equilibrium solidification of (a) sample 239 and (b) sample 239D.*

Table 2: *The proportions of phase formed during the solidification.*

Phase / Sample	239	239D
α-Al	87.00	85.20
β-Si (eutectic)	9.91	9.74
α-$Al_{15}(Fe,Mn)_3Si_2$	0.89	1.03
β-Al_5FeSi	1.31	3.26
Mg_2Si	0.86	0.65
Q-$Al_5Cu_2Mg_8Si_6$	0.02	0.11

220 °C and can be associated with the precipitation of the Q-$Al_5Cu_2Mg_8Si_6$ or Mg_2Si phase; a later point is not possible due to the very low copper content in the samples (239: 0.005 wt%; 239D: 0.0229 wt%). The second inflexion point represents T_S (239: 552.2 °C; 239D: 551.2 °C) and illustrates the onset of eutectic melting (α-Al + β-Si) with the Mg_2Si phase present. According to Thermo-Calc calculations, the next characteristic point (239: 565.5 °C; 239D: 563.7 °C) defines the melting of the eutectic (α-Al + β-Si) and the last characteristic temperature (239: 608.1 °C; 239D: 605.0 °C) represents the melting of the primary α-Al dendrites. On the cooling curves (blue), the first characteristic point is T_L (239: 575.5 °C; 239D: 569.4 °C), where the solidification of the primary α-Al dendrites begin. According to Thermo-Calc calculations, the next inflexion point is the solidification temperature of the eutectic (α-Al + β-Si) and the last one is the solidification of the eutectic (α-Al + β-Si + Mg_2Si) (239: 522.1 °C; 239D: 521.8 °C). In sample 239D, another inflexion point occurs at 544.3 °C, which most likely represents the eutectic solidification of the Fe-phases.

A light microscope was used to image the microstructure of all samples at various magnifications. Figures 5a and b show the microstructure of sample 239, while Figures 5c and d show sample 239D. According to the literature, the following microstructural components are observed in the microstructures in the figure: primary α-Al dendrites, binary eutectic (α-Al + β-Si), Fe-eutectic phase α-$Al_{15}(Fe,Mn)_3Si_2$ ('Chinese script'), needle shape β-Al_5FeSi phase, and the eutectic phase of Mg_2Si (black) [5]. Due to the presence of magnesium, the formation of the π-$Al_8FeMg_3Si_6$ phase is also possible [12]. Given the presence of strontium in the chemical composition of sample 239, the formation of the Al_2SrSi_2 phase can also be inferred [13]. The black arrows in Figures 5a and c indicate the deleterious β-Al_5FeSi phases, which are hardly observed in the microstructure of sample 239, while they are common in the microstructure of sample 239D. In sample 239, the eutectic (α-Al + β-Si) is much finer and rounder, which is due to the presence of strontium acting as a modifier of the eutectic β-Si.

Figures 6a and b show the microstructures of the as-cast and heat-treated sample 239 (239 and 239T). Figures 6c and d show the microstructures of the cast and heat-treated sample 239D (239D and 239DT). It can be observed that there is a visible decrease in the primary α-Al, according to the literature. A decrease in the eutectic (α-Al + β-Si) is observed especially for sample 239DT. As in the as-cast condition, the density of the β-Al_5FeSi phases in the heat-treated condition is much higher in the secondary alloy (239DT). After heat treatment, the thicker needles are rounded.

Figure 7 shows a comparison of the average hardness values between the qualities of alloys in the as-cast samples and after heat treatment. It can be seen that the hardness of sample 239 increases by ~ 28% and that of 239D alloy increases by ~ 42% after heat treatment. In general, the hardness of the as-cast sample 239D is ~ 6% higher than that of the purer alloy, and after heat treatment it is ~ 24% higher than that of the purer 239 sample.

Figure 8 shows a comparison of tensile test results between qualities of alloy and between the as-cast and heat-treated states. For better quality alloy, tensile strength and yield strength are increased by heat treatment, while elongation is greatly reduced by heat treatment. The alloy produced from secondary raw materials has significantly lower mechanical property values in the as-cast condition, and after heat treatment the material was so brittle that the mechanical properties could not be measured.

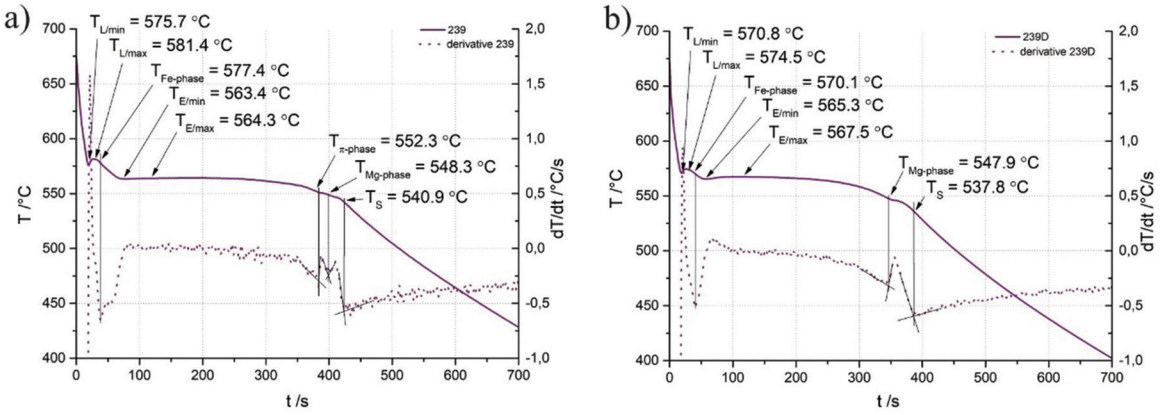

Figure 3: *The cooling curve and corresponding derivative of (a) sample 239 and (b) sample 239D.*

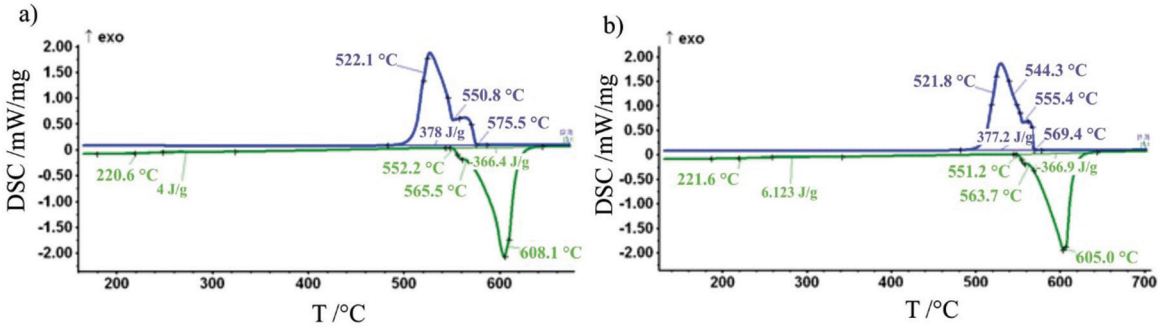

Figure 4: *Heating (green) and cooling (blue) DSC curve of the sample (a) 239 and (b) 239D.*

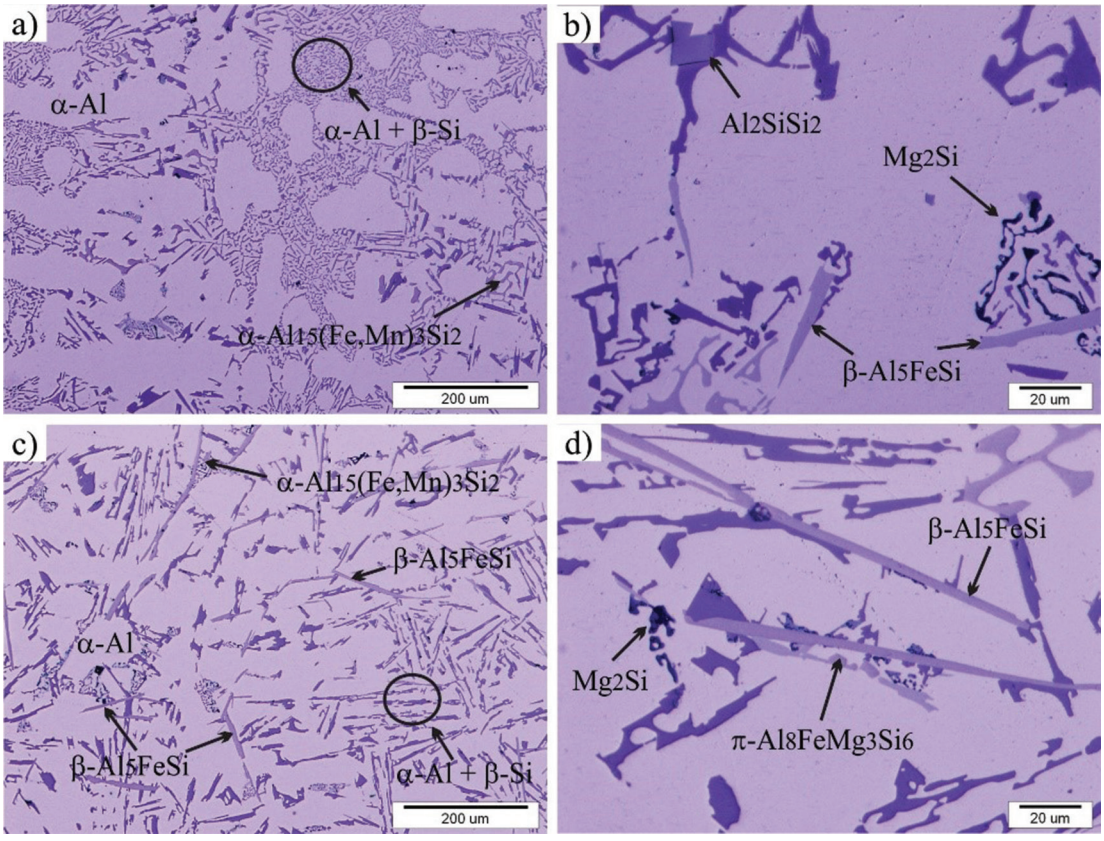

Figure 5: *Micrographs of (a and b) sample 239 and (c and d) sample 239D.*

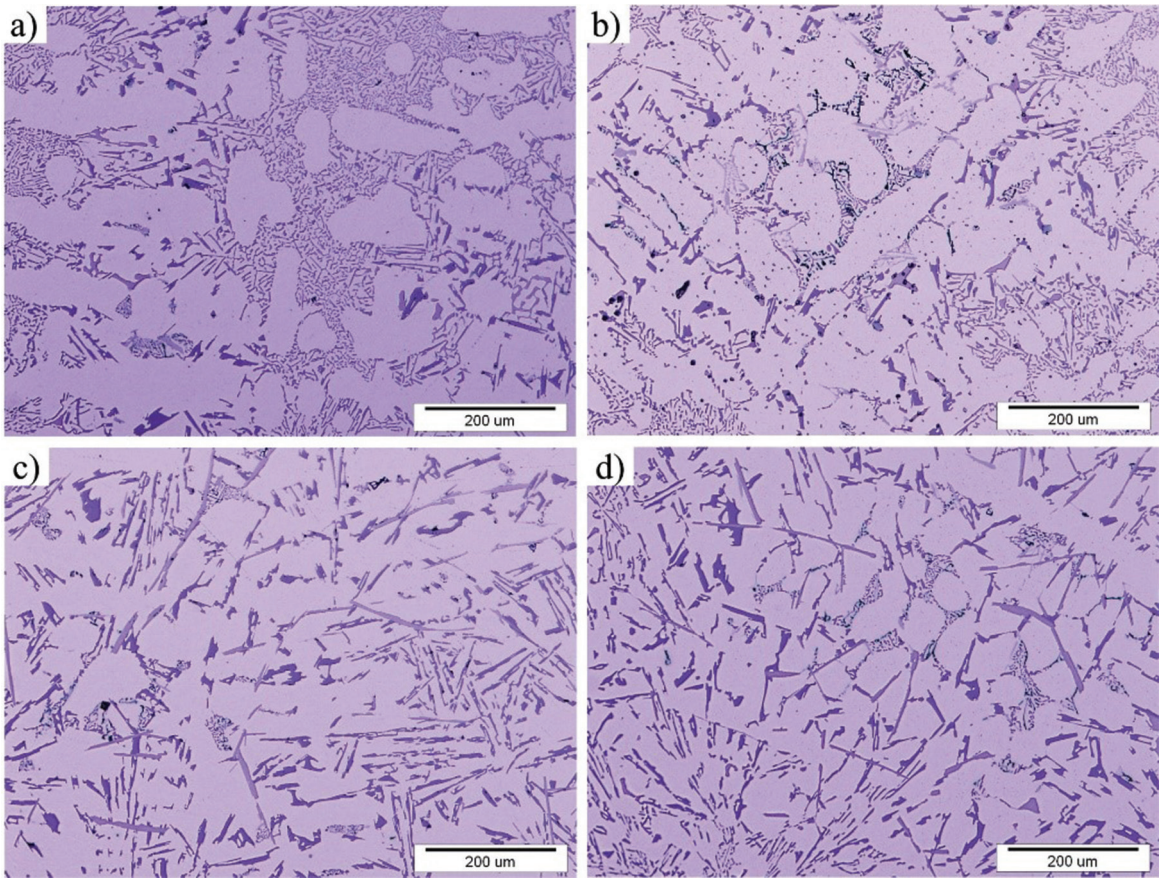

Figure 6: *Micrographs of sample 239 in (a) as-cast state and (b) T6 heat-treated state and of sample 239D (c) in as-cast state and (d) T6 heat-treated state.*

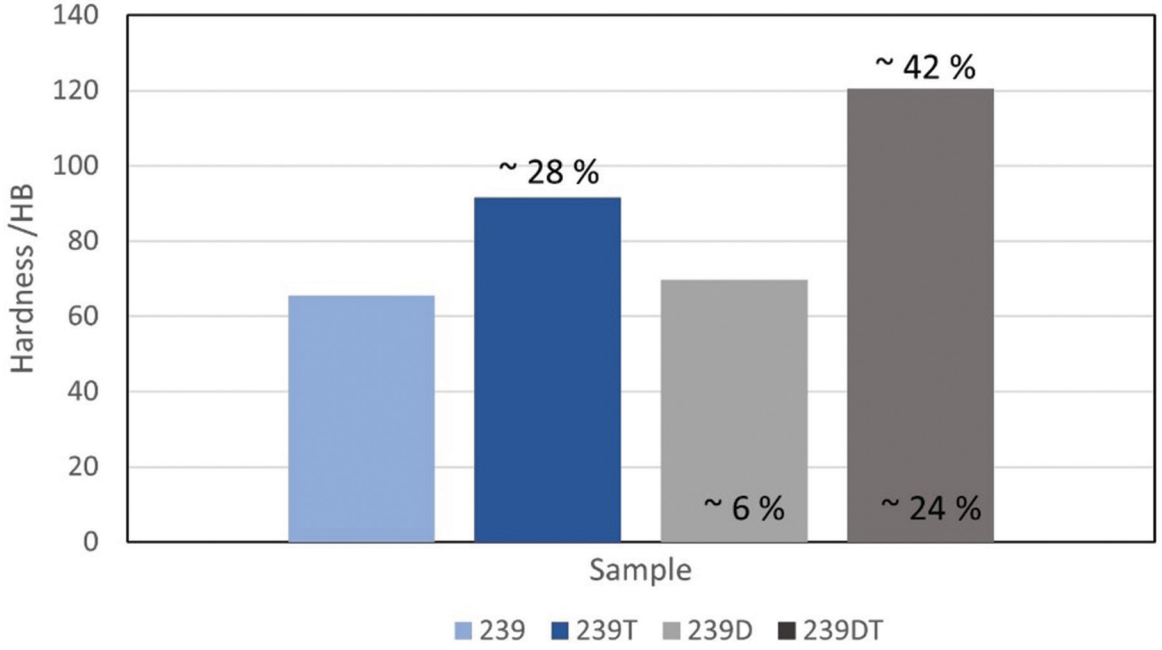

Figure 7: *Hardness of AlSi10Mg alloy and AlSi10Mg(Fe) alloy in as-cast state and after heat treatment.*

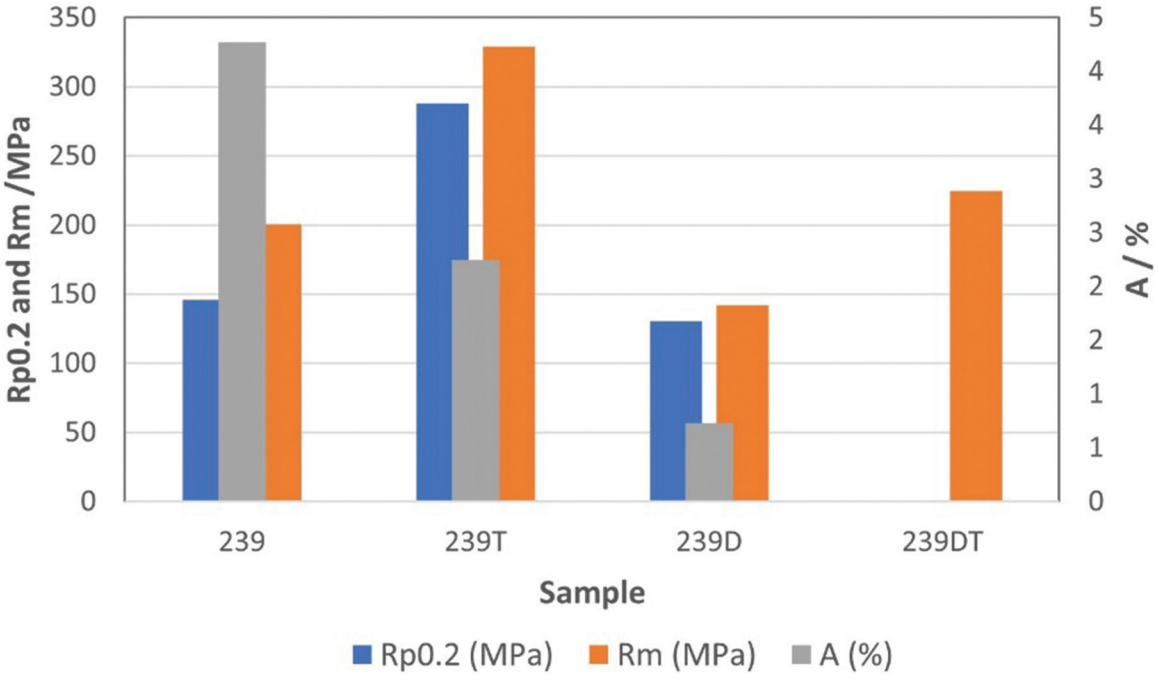

Figure 8: *Tensile test results for 239 alloys and 239D alloys in the as-cast state and after heat treatment.*

Conclusion

Thermal analysis methods can give us an important and necessary indication of the quality of the alloys used.

Recycling aluminium is the future from an energy point of view. Therefore, it is important to produce high quality alloys from secondary raw materials that can replace those produced from primary aluminium.

The deleterious β-Al_5FeSi phases were hardly observed in the microstructure of the purer sample, while they are common in the microstructure of inferior quality sample. A visible decrease in the primary α-Al and in the eutectic (α-Al + β-Si) was observed, especially for samples of inferior quality after heat treatment. As in the as-cast condition, the density of the β-Al_5FeSi phases in the heat-treated condition is much higher in the alloy of inferior quality. After heat treatment, the thicker needles are rounded. In general, the hardness of the as-cast sample of inferior quality was ~ 6% higher than that of the purer alloy and after heat treatment was ~ 24% higher than that of the purer sample. For better quality alloy, tensile strength and yield strength are increased by heat treatment, while elongation is greatly reduced by heat treatment. The alloy produced from secondary raw materials has significantly lower mechanical property values in the as-cast condition.

The analysis of the effects of alloy quality of primary and secondary produced AlSi10Mg alloys on solidification, microstructure and mechanical properties revealed significant differences in the results of the analysed properties. Based on the results, we can predict when it is appropriate to use a primary produced alloy with higher purity and when to use a secondary produced alloy with more and higher concentration of alloying elements.

Acknowledgement

The work was co-financed by the Republic of Slovenia, the Ministry of Education, Science and Sport, and the European Regional Development Fund. The work was carried out in the framework of the project Modelling of Thermomechanical Processing of the Aluminium Alloys for High Quality Products (MARTIN, Grant No.: C3330-18-952012).

References

[1] Yildirim, M., Özyürek, D. (2013): The effects of Mg amount on the microstructure and mechanical properties of Al-Si-Mg alloys. *Materials & Design*, 51, pp. 767-774, DOI:10.1016/j.matdes.2013.04.089.

[2] Kaufman, J.G., Rooy, E.L. (2004): *Aluminium alloy castings: Properties, processes, and aplications*. ASM International, 340 p.

[3] SS-EN 1676:2010. *Aluminium and aluminium alloys - Alloyed ingots for remelting – Specifications* [cited 20/10/2020]. Available on: *https://www.stenaaluminium.com/siteassets/document/product-sheets/eng-en-ab-43400.pdf*.

[4] Raffmetal the Aluminium Evolution. Continuous casting alloys: EN AB 43000 AlSi10Mg(Fe) alloy [cited 11/7/2020]. Available on: *https://www.raffmetal.com/web_eng/prodotti.asp?q=1*.

[5] Vončina, M., Medved, J., Mrvar, P. (2005): Thermodynamic analysis of MgSi10Mg alloy. *RMZ – Materials and Geoenvironment*, 52(3), pp. 621–633.

[6] Que, Z., Wang, Y., Fan, Z. (2018): Formation of the Fe-containing intermetallic compounds during solidification of Al5Mg2Si0.7Mn1.1 Alloy. *Metallurgical and Materials Transactions A*, 49, pp. 2173–2181, DOI: 10.1007/s11661-018-4591-6.

[7] Ravi, M., Mech, K., Sasidharan, V., et al. (2014): Influence of alloying elements and casting process on the mechanical properties of al-si piston alloy. *National conference on advances in materials and advances in bioprocess engineering. At: Mohandas College of Engineering and technology.*

[8] Girelli, L., Tocci, M., Gelfi, M., Pola, A. (2019): Study of heat treatment parameters for additively manufactured AlSi10Mg in comparison with corresponding cast alloy. *Materials Science & Engineering A,* 739, pp. 317–328, DOI: 10.1016/j.msea.2018.10.026.

[9] Zyguła, K., Nosek, B., Pasowiec, H., Szysiak, N. (2018): Mechanical properties and microstructure of AlSi10Mg alloy obtained by casting and SLM technique. *World Scientific News*, 104, pp. 462–472, DOI: 10.1007/s12633-021-01340-9.

[10] Bäckerud, L., Chai, G., Tamminen, J. (1990): *Solidification characteristics of aluminium alloys. Volume 2, foundry alloys.* AFS/SKANALUMINIUM: Stockholm, 266 p.

[11] Medved, J., Kores, S., Balaško, T., Vončina, M. (2019): Influence of minor alloying element addition on aluminium casting alloys, *Livarski vestnik,* 66(3), pp. 191-202.

[12] Vončina, M., Medved, J., Kores, S., Xie, P., Schumacher, P., Li, J. (2013): Precipitation microstructure in Al-Si-Mg-Mn alloy with Zr additions. *Materials characterization*, 155, 8 p., DOI: 10.1016/j.matchar.2019.109820.

[13] Petrič, M. (2013): *Sprememba dimenzij in električne upornosti med strjevanjem litin iz sistema Al-Si.* Ph. D. Thesis. University of Ljubljana, Faculty of Natural Sciences and Engineering, Department of Materials and Metallurgy: Ljubljana, 138 p.